

1 **Assessing the Convective Environment over Irrigated and Non-**
2 **Irrigated Land Use with Land-Atmosphere Coupling Metrics:**
3 **Results from GRAINEX**

4
5 (Submitted to: *Journal of Hydrometeorology*)

6
7 Daniel Whitesel^{1, 2, 3}, Rezaul Mahmood^{1, 3, *}, Christopher Phillips⁴, Joshua Roundy⁵, Eric
8 Rappin⁶, Paul Flanagan⁷, Joseph A. Santanello Jr.⁸, Udaysankar Nair⁴, and Roger Pielke, Sr.⁹

9
10 ¹High Plains Regional Climate Center and ²National Drought Mitigation Center, ³School of
11 Natural Resources, University of Nebraska-Lincoln, Lincoln, NE

12
13 ⁴Department of Atmospheric Science, University of Alabama in Huntsville, Huntsville, AL

14
15 ⁵Department of Civil, Environmental, and Architectural Engineering, University of Kansas,
16 Lawrence, KS

17
18 ⁶Kentucky Climate Center, Western Kentucky University, Bowling Green, KY

19
20 ⁷U.S. Department of Agriculture-Agricultural Research Service, El Reno, OK

21
22 ⁸Hydrological Sciences Laboratory, NASA GSFC, Greenbelt, MD

23
24 ⁹Department of Atmospheric and Oceanic Sciences and CIRES, University of Colorado-Boulder,
25 Boulder, CO

26
27
28 *Corresponding Author: rmahmood2@unl.edu

31 **Abstract**

32
33 Land use land cover change affects weather and climate. This paper quantifies land-
34 atmosphere interactions over irrigated and non-irrigated land uses during the Great Plains
35 Irrigation Experiment (GRAINEX). Three coupling metrics were used to quantify some land-
36 atmosphere interactions as it relates to convection. They include: the Convective Triggering
37 Potential (CTP) and Low-Level Humidity Index (HI_{low}), and the Lifting Condensation Level
38 (LCL) Deficit. These metrics were calculated from the rawinsonde data obtained from the
39 Integrated Sounding Systems (ISS) for Rogers Farm and York Airport along with soundings
40 launched from the Doppler on Wheels (DOW) sites. Each metric was categorized by Intensive
41 Observation Period (IOP), cloud cover, and time of day.

42 Results show that with higher CTP, lower HI_{low} , and lower LCL Deficit, conditions were
43 more favorable for convective development over irrigated land use. When metrics were grouped
44 and analyzed by IOP, compared to non-irrigated land use, HI_{low} was found to be lower for
45 irrigated land use suggesting favorable conditions for convective development. Furthermore,
46 when metrics were grouped and analyzed by clear and non-clear days, CTP values were higher
47 over irrigated cropland compared to non-irrigated land use. In addition, compared to non-
48 irrigated land use, LCL Deficit during the peak growing season was lower over irrigated land
49 use, suggesting favorable condition for convection. It is found that with the transition from the
50 early summer to the mid/peak summer and increased irrigation, the environment became more
51 favorable for convective development over irrigated land use. Finally, it was found that
52 regardless of background atmospheric conditions, irrigated land use provided a favorable
53 environment for convective development.

59 **1. Introduction and Background**

60 Land use land cover change (LULCC) is an important driver of regional weather and
61 climate (Pielke et al. 2011; Mahmood et al. 2010, 2014; Cook et al. 2020; McDermid et al.
62 2023). Human activities such as deforestation, urbanization, and agriculture, are the main drivers
63 of LULCC. LULCC impacts the surface energy balance, moisture budgets, and other land
64 surface properties (Pielke et al. 2016), which can lead to changes in local and regional
65 atmospheric circulations, temperature, and precipitation (Mahmood et al. 2004, 2006, 2011,
66 2013; Shukla et al. 2014; Fan et al. 2015a, b; Xu et al. 2015; Mueller et al. 2016, 2017;
67 Winchester et al. 2017; Singh et al. 2018; Rodgers et al. 2018; Chen and Dirmeyer 2019; Nair et
68 al. 2019; Zhang et al. 2019; Hu et al. 2019; Flanagan et al. 2021; McDermid et al. 2021; Rappin
69 et al. 2021, 2022; Phillips et al. 2022).

70 Irrigated agriculture is in high demand, due to the increasing need for food (McDermid et
71 al. 2023). Two effects are found to be common with irrigation's application: an increase in
72 evapotranspiration (ET) and a decrease in air temperatures (Mahmood and Hubbard 2002, 2004,
73 2006, 2013; DeAngelis et al. 2010, Cook et al. 2011, 2015, 2020; Sen Roy et al. 2007, 2011;
74 Alter et al. 2015, 2018; Pei et al. 2016; McDermid 2019; Yang et al. 2019; Rappin et al. 2021).
75 With an increase in ET comes increases in latent and decreases in sensible heat fluxes, thereby
76 changing the surface energy balance (Mahmood et al. 2013; Rappin et al 2021). The decrease in
77 sensible heat flux results in lower maximum air temperatures. Analysis of long-term observed
78 temperature data-based studies suggest that over the Great Plains, compared to non-irrigated
79 areas and during the growing season, irrigation resulted in 1.01 °C cooling of mean maximum
80 temperature (Mahmood et al. 2004, 2006, 2013) In addition, Bonfils and Lobell (2007) found
81 ~ 0.20 °C decade⁻¹ cooling trends in temperature over irrigated areas during growing season in
82 Nebraska. Analysis of growing season observed data found up to 2.17 °C increased dew point
83 temperatures over irrigated areas (Mahmood et al. 2008). In an observational data-based study
84 for California Christy et al. (2006) found a 0.26 °C per decade cooling of growing season
85 maximum temperature due to irrigation. In a subsequent study, Lawston et al. (2020) found up
86 1.68 °C cooling of mean maximum summer temperature in the Pacific Northwestern U.S. due to
87 irrigation. Furthermore, historical observed data analysis suggests up to 0.34 °C cooling of
88 growing season maximum temperatures over irrigated areas in India (Sen Roy et al. 2007). The
89 same study found up to 0.53 °C cooling of temperature during individual growing season

90 months. In a recent research, Kang and Eltahir (2019) found that the surface temperature
91 decreased by 0.43 °C due to irrigation in the North Central Plains of China.

92 However, its effects on precipitation are more complex. An observational data-based
93 study suggests that precipitation can be reduced in the immediate area due to the decrease in
94 sensible heat lowering the likelihood of cloud formation by reducing turbulent transfer (Szilagyi
95 and Franz, 2020). Furthermore, observed historical data suggests that in regions downwind,
96 irrigation can potentially increase precipitation (Barnston and Schickedanz 1984). Sen Roy et al.
97 (2011) found up to 69 mm (121%) increase in total precipitation for growing seasons due to
98 irrigation in the northwestern India. It is also found that over North China Plains precipitation
99 increased 1.25 mm day⁻¹ after the full implementation of irrigation (Kang and Eltahir 2019).

100 Irrigation increases soil moisture, and a significant amount of research has been
101 conducted in the past focusing on soil moisture and its role in L-A interactions (e.g., Ookouchi et
102 al. 1984; Eltahir 1998; Findell and Eltahir 2003a, b; Leeper et al. 2011; Mahmood et al. 2012;
103 Suarez et al. 2014; Santanello et al. 2018). These studies assessed, among others, the evolution
104 of the planetary boundary layer (PBL) and related boundary layer processes, the role of surface
105 fluxes in the PBL development, and changes in various convective parameters such as the LCL
106 and the LFC. Soil moisture impacts the surface energy and water budgets through changes to the
107 albedo and Bowen ratio (the ratio of the surface sensible heat flux to the latent heat flux, or ET)
108 or evaporative fraction (EF, ratio of the latent heat flux to the net surface flux (i.e. net radiative
109 flux)). The wetter the soil, the greater the amount of incoming radiational energy is partitioned
110 into ET, leading to relatively smaller values of atmospheric sensible heat flux and a larger EF.
111 Depending on the specific humidity of the PBL, ET from moist soil can be static or change in
112 magnitude over multiple time scales. For example, as ET occurs and the PBL moistens, the
113 magnitude of EF reduces. Large-scale circulations can therefore have a significant impact on a
114 process chain for L-A interactions proposed by Santanello et al. (2018) where moist (dry)
115 advection over wet soil can reduce (increase) the magnitude of ET. On the other hand, it is the
116 soil moisture that controls the partitioning between sensible and latent heat fluxes. When soils
117 are wet, the latent heat flux is determined by the available net radiation and latent heat fluxes
118 dominate. Whereas when the soil is dry, the availability of moisture controls the degree of latent
119 heating, which is depressed at the expense of sensible heat fluxes.

120 Just as soil moisture (from irrigation or precipitation) exerts a strong control on the EF,
121 the EF exerts a strong control on the PBL's growth and decay. Low values of EF (e.g., large
122 sensible heat flux) supports PBL growth while a large EF will significantly reduce PBL growth
123 due to a weak buoyant heat flux. In summary, sensible heating and small EF help to grow the
124 PBL while latent heating moistens the PBL but may not necessarily grow it to the LCL. The role
125 of surface fluxes and their influence on the PBL structure and evolution were further discussed
126 by Santanello et al. (2007, 2009, 2011, 2013, 2018, and 2019). This understanding is further
127 supported by McPherson (2007), as she noted that the strength of land-atmosphere interactions is
128 sensitive to potential ET and surface physical conditions including soil moisture. Holt et al.
129 (2006) suggested that the modification of soil moisture (e.g., by irrigation) changes emissivity
130 and albedo which subsequently affects L-A interactions via changes in sensible and latent energy
131 partitioning, air temperature, and PBL moisture content. The response propagates upward
132 through the boundary layer via turbulent transport and affects boundary layer growth, convective
133 initiation, and precipitation amounts.

134 It is noted that wet soils can lead to a shallow boundary layer and a large moist entropy
135 per unit mass (Eltahir 1998). As a result, a low LFC combined with high boundary layer specific
136 humidity may result in a positive soil moisture/evaporative – cloud formation feedback.
137 Conversely, over regions of dry soil the sensible heat flux dominates the latent heat flux (large
138 Bowen ratio) and can hinder cloud development. Overall, given the existence of both positive
139 and negative soil moisture-cloud development feedback, it is not surprising that both positive and
140 negative soil moisture-precipitation (hence, irrigation-precipitation) feedbacks have also been
141 identified (e.g., Ford et al. 2015a, b). The positive feedback, in which precipitation forms
142 preferentially over wet soils has been found in one-dimensional idealized models (Eltahir 1998,
143 Findell and Eltahir 2003a, b, c) as well as in three dimensional mesoscale models (Schlemmer
144 2011, 2012) and observations (Betts and Ball 1998; Taylor 2010; and Berg et al. 2013).

145 The entire process link chain proposed by Santanello et al. (2018) is bookmarked by the
146 relationship between soil moisture and precipitation, termed the soil moisture-precipitation (SM-
147 P) feedback (or termed as irrigation-precipitation for our purpose). There are numerous
148 complexities to local soil moisture-ET-convective initiation-precipitation feedback. Furthermore,
149 a relatively large Bowen ratio leads to a deep boundary layer and elevated LCL. In the absence
150 of sufficient moisture, the LFC will not descend to the lifting condensation level and shallow

151 convection as opposed to deep convection will develop. On the other hand, irrigation induced
152 increases in soil moisture would result in stronger latent energy fluxes and a smaller Bowen
153 ratio. These factors would result in a shallow boundary layer with large moist static energy such
154 that subsequent large-scale forcing would lead to significant additional precipitation.

155 Research suggests that thunderstorm severity may be enhanced due to differential heating
156 between areas of moist and adjacent dry, vegetated land (Segal et al. 1988; Pielke and Zeng
157 1989). Moreover, soil moisture enhancement due to agriculture and irrigation significantly
158 impacts weather and climate (e.g., Puma and Cook 2010; Wei et al. 2013). Excellent examples of
159 the impacts of increased soil moisture due to irrigation can be found in the GP of North America
160 (Barnston and Schickendanz 1984; Mahmood and Hubbard 2002; Adegoke et al. 2003;
161 DeAngelis et al. 2010; Harding et al. 2012a, b; and Lawston et al. 2015).

162 Irrigation induced increases in soil moisture can also be a good indicator of the location
163 of deep convection (Findell & Eltahir 2003a, b; Frye and Mote 2010). Findell and Eltahir (2003a,
164 b) utilized the Convective Triggering Potential (CTP) and Low-Level Humidity Index (HI_{low}) to
165 determine where deep convection would initiate with respect to soil moisture, using morning
166 balloon sounding data. Additionally, studies suggest that there is a negative relationship between
167 soil moisture and Lifting Condensation Level (LCL) Deficits (Santanello et al. 2011) In other
168 words, wetter soils lead to lower LCL Deficits compared to drier soils. This can provide
169 favorable conditions for cloud formation over wetter soils, even with the reduction of turbulent
170 transfer over wetter soils.

171 In this context, the Great Plains Irrigation Experiment (GRAINEX) aimed to better
172 understand land-atmosphere (L-A) interactions between irrigated and non-irrigated cropland
173 (Rappin et al. 2021). It was found that irrigated land use lowers near surface maximum air
174 temperature, increases dew point temperature, lowers planetary boundary layer heights (PBLH)
175 and produces higher latent and lower sensible heat fluxes compared to non-irrigated cropland
176 (Rappin et al. 2021, 2022; Lawston-Parker et al. 2023; Lachenmeier et al. 2024). Further analysis
177 of GRAINEX data found that the irrigated land use weakens baroclinicity and meso-scale
178 upslope circulations in the Great Plains (GP) and potentially influences the GP Low Level Jet
179 (Phillips et al. 2022).

180 The overall goal of this paper is to further understand the changes in the convective
181 environment over irrigated and non-irrigated land uses by utilizing three coupling metrics. These

182 metrics include CTP, HI and LCL Deficit (Findell and Eltahir 2003a, b; Ferguson and Wood,
183 2011; Santanello et al. 2018). These metrics allowed us to identify environments favorable for
184 convection. *A key advantage of the current study is the use of a large number of radiosonde*
185 *observations launched throughout the day including the typical periods of convective*
186 *development. These launches were conducted during two distinct periods of crop/vegetation*
187 *growth and irrigation application. Findell and Elathir (2003a, b) used morning only soundings in*
188 *conjunction with a modeling framework while Ferguson and Wood (2011) primarily used*
189 *satellite data to explore L-A interactions. As such, this work provides a new perspective in L-A*
190 *interactions over irrigated and non-irrigated land uses and soil moisture gradients (wet-dry)*
191 *utilizing in-situ observations. In addition, this research is complementary to Lachenmeier et al.*
192 *(2024) where the authors investigated impacts of irrigation on the planetary boundary layer*
193 *height (PBLH), LCL, Level of Free Convection (LFC), and PBL mixing ratio. It is found that*
194 *irrigation lowers PBLH, LCL, and LFC and increases PBL mixing ratio.*

195 In the context of these interactions between the land and atmosphere and the objectives of
196 this research, the following sections of the paper provide further background on L-A interactions,
197 discuss data used from the GRAINEX, methods applied to data, results, analysis and assessment
198 of the findings, and conclusions.

199

200 **2. Data and Methods**

201 *a. The GRAINEX Field Campaign and Observations*

202 A detailed description of the GRAINEX field campaign, collected data, and the
203 observation platforms used are provided in Rappin et al. (2021). Hence, only a brief description
204 is provided here. Data collection was completed during late May through early August of 2018
205 over southeast Nebraska. Specifically, the field campaign was completed across two 15-day
206 periods during the growing season of 2018; from May 30 through June 13, known as the
207 Intensive Observation Period 1 (IOP1) and from July 16 through July 30, known as the Intensive
208 observation Period 2 (IOP2) in 2018. Nebraska, located in the northern part of the North
209 American GP, is one of the most extensively irrigated regions in the world (Bonfils and Lobell
210 2007; Lobell et al. 2009). In southeast Nebraska (Figure 1), non-irrigated land use (eastern part
211 of the study area) transitions to irrigated land use (western part of the study area) as water from

212 the High Plains Aquifer becomes available for extraction. This transition also follows the east to
213 west declining precipitation gradient of the North American GP. Note that Nebraska is located
214 within the GP. Common crops in the study area are corn and soybeans. During the field
215 campaign, both IOP1 (late spring/beginning of the summer) and IOP2 (mid-summer)
216 experienced several rain events and periods of cooler and drier days (Rappin et al. 2021).

217 Data collection was completed by using a variety of observational platforms including 12
218 eddy covariance Integrated Surface Flux Systems (ISFS) (UCAR/NCAR 1990), two Integrated
219 Sounding Systems (ISS) (UCAR/NCAR 1997), three Doppler on Wheels (DOW) mobile radar
220 units (Wurman et al. 2021), and 75 Environmental Monitoring, Ecological Sensor Hubs
221 (EMESH) (Rappin et al. 2021). In addition, a Twin Otter aircraft mounted with radiometers, was
222 flown over the study area by the National Aeronautical and Space Administration (NASA),
223 which collected soil moisture data. Our current paper focuses on data from the ISS and DOW.
224 Thus, discussion on data from ISFS, EMESH and NASA is not provided.

225

226 *b. Integrated Sounding Systems (ISS)*

227 As noted previously, there were two ISS sites from where rawinsonde balloons were
228 launched throughout IOP1 and IOP2. Land use around one ISS site (ISS3 at York) was irrigated
229 agriculture while for the other one (ISS2 at Rogers Farm) was non-irrigated agriculture. For
230 each location, the first balloon was launched around 5:00 AM Local Standard Time (LST) [6:00
231 AM Local Time (LT); 1100 UTC] and the last launch was around 7:00 PM LST (8:00 PM LT;
232 0100 UTC, next day). They were launched simultaneously every two hours and every day during
233 IOP1 and IOP2. Hence, sixteen balloons were launched every day and overall, 480 launches (8
234 launches x 2 sites x 30 days) were completed from the two sites. In short, this field campaign
235 provided the most comprehensive data set of this type for investigation into of the impacts of
236 land use, including irrigation, on the atmosphere.

237

238

239

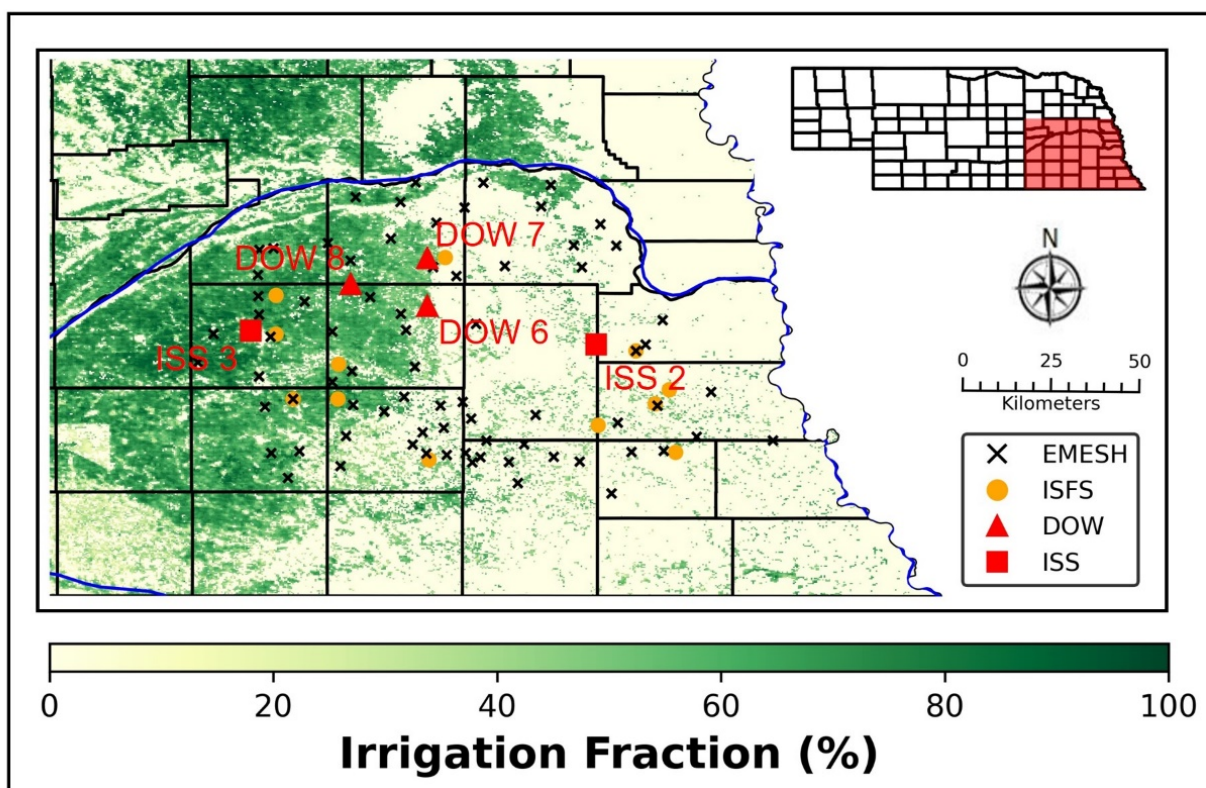
240

241

242

243 *c. Doppler on Wheels (DOW)*

244 Rawinsondes from three DOW locations were also launched simultaneously with the ISS
245 launches (8 launches x 3 sites x 30 days = 720 launches). In total about 1200 rawinsonde
246 launches (ISS + DOW sites) were completed. DOW8 was located over irrigated land use, DOW
247 7 was over non-irrigated, and DOW6 was in a transitional area. For additional details regarding
248 all observation platforms and instrumentation, please consult Rappin et al. (2021) and
249 https://www.eol.ucar.edu/field_projects/grainex.



250
251 Figure 1. Map of the GRAINEX study area in southeast Nebraska. Data collection sites consisted
252 of 12 integrated surface flux system sites (ISFS), two integrated sounding system sites (ISS),
253 three Doppler on Wheels deployment locations (DOW), and 75 Environmental Monitoring,
254 Economical Sensor Hubs (EMESH).

255
256
257
258

259 *d. Calculation of Convective Triggering Potential, Low-Level Humidity Index, and LCL Deficit*

260 Calculations of CTP, HI_{low} , and LCL Deficit were completed for ~1050 soundings from
261 the two ISS locations and the three DOW locations (EOL 2020). This study was focused on the
262 morning [0700 AM-1100 AM Local Standard Time (LST) (1300-1700 UTC)] and afternoon
263 [0100 PM-0700 PM LST (1900-0100 UTC) when L-A interactions can be effectively captured
264 by the rawinsonde dataset. The formulation from Ferguson and Wood (2011) was used to
265 calculate CTP and HI_{low} . These metrics were originally designed for morning soundings to
266 capture the boundary layer properties prior to the onset of daytime land surface fluxes and to
267 address the limitations of sounding launch frequency from the National Weather Service (one in
268 the morning and one in the late afternoon). However, the wealth of sounding data from
269 GRAINEX allowed for calculation of CTP and HI_{low} every two hours, which provides a unique
270 perspective of how CTP and HI_{low} evolve during the day. Ferguson and Wood (2011) defined
271 CTP ($J\ kg^{-1}$) as the integral of the area between the temperature sounding profile, T_{env} (K), and a
272 moist adiabat, T_{parcel} (K), raised from the observed temperature and humidity 100 hPa (~1 km)
273 above ground level (AGL) to a level 300 hPa (~3 km) AGL. AGL CTP can be expressed as
274 follows:

275

$$276 \quad CTP = g \int_{Z_{PSurfStd-300}}^{Z_{PSurfStd-100}} \left(\frac{T_{parcel} - T_{env}}{T_{env}} \right) dz \quad (1)$$

277 In this equation (1) g is the gravitational acceleration ($9.807\ m\ s^{-2}$) and dz is the thickness (m) of
278 the layer.

279 Based on equation 1, it can be stated that the CTP assists in understanding lower
280 tropospheric stability by measuring the departure of the temperature profile from moist adiabatic
281 conditions in the region between 100 and 300 hPa (~1-3 km) AGL (Findell and Elathir 2003a, b;
282 Santanello et al. 2018). When the actively growing daytime PBL reaches the level of free
283 convection (LFC), deep convection can develop with sufficient moisture. For convective
284 triggering, it is noted that PBL moistening and a simultaneous rapid lowering of the LFC is a
285 more effective mechanism for convective development when the lower atmosphere is near moist
286 adiabatic, and CTP is low (Santanello et al. 2018). On the other hand, high sensible heat flux and
287 rapid PBL growth is more effective for convection development when the low-level atmospheric

288 profile is near dry adiabatic, and the CTP is high. Overall, a negative CTP suggests that the local
289 atmosphere is too stable for convection to develop (Findell Eltahir 2003a).

290 Subsequently, following the formulation of Ferguson and Wood (2011), HI_{low} is
291 calculated as the sum of the dewpoint depressions at 50 and 150 hPa pressure AGL and can be
292 expressed as follows:

$$293$$
$$294 HI_{low} = (T_{PSurfStd-50} - T_{d,PSurfStd-50}) + (T_{PSurfStd-150} - T_{d,PSurfStd-150}) \quad (2)$$

295 Here (equation 2), $T_{PSurfStd-p}$ and $T_{d,PSurfStd-p}$ are the temperature and dewpoint temperature at
296 pressure p AGL, respectively.

297 When HI_{low} indicates that when lower atmosphere is extremely dry (higher value of
298 HI_{low}), then moisture from the surface evaporated into the PBL will not be available for
299 sufficiently enhancing the moist static energy of the PBL for convection to occur (Findell and
300 Eltahir 2003a, b; Santanello et al 2018). These types of days are identified as atmospherically
301 controlled when rain cannot be initiated by local surface processes. Likewise, if the HI_{low} is close
302 to zero, it is also atmospherically controlled due to a very moist atmosphere which will likely
303 lead to convection regardless of land surface controls. Note, that lower HI_{low} values suggest a
304 moister environment. Various ranges of favorable HI_{low} for different underlying conditions are
305 provided in Table 1 in the following section.

306 The LCL Deficit is the difference between the Lifting Condensation Level (LCL) and the
307 Planetary Boundary Layer height (PBLH). This metric was designed to measure the deficiencies
308 in the growth of the planetary boundary layer due to a lack of mixing of heat and moisture
309 (Santanello et al 2011). Larger LCL Deficit values indicate such deficiencies in the PBL growth.
310 However, when the LCL Deficit is zero or negative, the PBL has developed past the LCL and
311 clouds will readily form within the PBL. During wet coupling PBLH and LCL both can be
312 lowered and result in smaller LCL Deficits due to higher latent and lower sensible heat flux over
313 irrigated areas and provide conditions for convection, cloud development, and precipitation.
314 Under dry coupling, the LCL Deficit can be lower due to higher PBLH linked to an increase in
315 sensible heat flux (Roundy and Santanello 2017). LCL Deficits were calculated every two hours
316 along with CTP and HI_{low} .

317

318 *e. CTP-HI_{low} Framework and LCL Deficit*

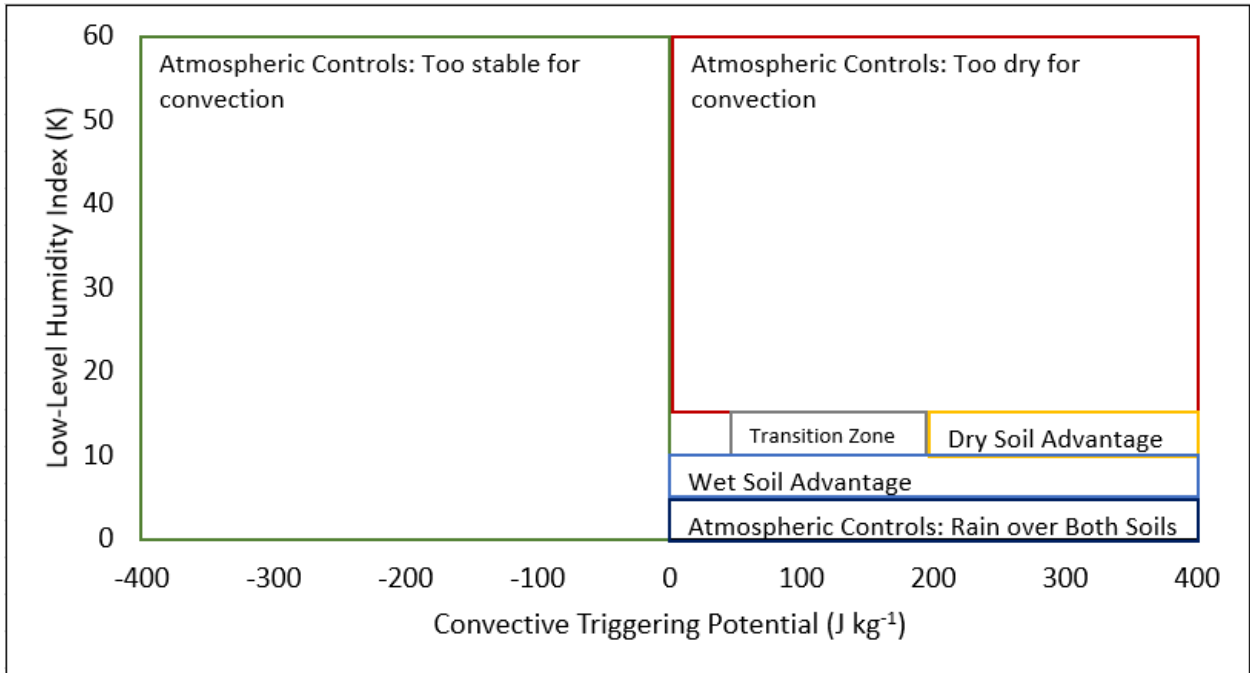
319 CTP values and corresponding HI_{low} values were categorized following the framework of
 320 Findell and Eltahir (2003a) and presented in Table 1. To further illustrate their role in L-A
 321 interactions they are also presented graphically in Figure 2.

322 Table 1. CTP-HI_{low} framework categories (following Findell and Eltahir 2003a).

| Category | Conditions | Box Color |
|--|--------------------------------------|-----------|
| Atmospherically Controlled; too dry for rain | $CTP > 0, HI_{low} \geq 15$ | Red |
| Atmospherically Controlled; too stable for rain | $CTP < 0$ | Green |
| Atmospherically Controlled; precipitation occurs in both wet and dry soils | $CTP > 0, 0 < HI_{low} < 5$ | Dark Blue |
| Transition Zone | $50 < CTP < 200, 10 < HI_{low} < 15$ | Grey |
| Wet Soil Advantage | $CTP > 0, 5 < HI_{low} < 10$ | Blue |
| Dry Soil Advantage | $CTP > 200, 10 < HI_{low} < 15$ | Yellow |

323
 324
 325
 326
 327
 328
 329
 330
 331
 332
 333
 334
 335
 336

337 These categories presented in table 1 can further be presented as follows:



338
339 Figure 2. CTP- HI_{low} framework categories (following Findell and Eltahir 2003a).

340
341 Subsequently, CTP and HI_{low} were analyzed along with LCL Deficit for irrigated and non-
342 irrigated land uses for IOPs (i.e., IOP1 and IOP2), cloud cover (clear and non-clear days), clear
343 and non-clear days over IOP1 and IOP2, time of day (morning and afternoon), morning and
344 afternoon over clear and non-clear days, and for morning and afternoon over clear and non-clear
345 day for IOP1 and IOP2 (Table 2). Clear days were first identified using MODIS Aqua and Terra
346 cloud fraction of less than 20%. MODIS Terra’s orbit carries it south-to-north over the equator at
347 approximately 10:30 local, and Aqua follows 3 hours after at 13:30 local. Thus, there are three
348 hours between the two satellite observations, and they are concentrated in the afternoon when
349 boundary layer is deepest. To ensure that other times during the day were consistently low-cloud
350 cover, GOES 16 satellite data from the NASA worldview (NASA 2021) was manually
351 examined. When considering the shallow cumuli, the same threshold was applied, and days that
352 produced deep convection were not counted as clear days. The rationale for including shallow
353 cumuli despite potential shading effects is that they are indicative of a convectively active PBL,
354 and restricting the cloud cover further leaves very few days upon which to conduct analysis. This
355 methodology has been used successfully in other GRAINEX studies (e.g., Phillips et al. 2022).

356 After applying these criteria, we have found five clear days during IOP1 and four in IOP2 (total
 357 9 days). The remaining 21 days were classified as non-clear days. Statistical significance tests (*t*-
 358 test) were completed with a 95% confidence level. Subsequently, *t*-tests were completed with a
 359 90% confidence level to communicate additional important findings which did not meet 95%
 360 confidence level requirement. Again, note that this study collected and analyzed a large amount
 361 of data, representing wide variety of conditions through a large sampling of the atmosphere
 362 (1200 radiosonde launches in 30 days; 40 per day) so that the objectives of the experiment can be
 363 met.

364

365 Table 2. Analysis and grouping of coupling metrics for different conditions to assess L-A
 366 interactions over irrigated and non-irrigated land uses.

| Category | Additional description |
|---|--|
| IOP1 and IOP2 | Regardless of cloud cover (clear vs. non-clear days) and time of day (morning vs. afternoon) |
| Cloud cover: Clear vs. non-clear days | Regardless of time of season (IOP1 and IOP2) and time of day (morning vs. afternoon) |
| Cloud cover: Clear vs. non-clear days during IOP1 and IOP2 | Regardless of time of day (morning vs. afternoon) |
| Time of Day | Regardless of time of season (IOP1 and IOP2) and cloud cover (clear vs. non-clear days) |
| Time of Day (morning vs. afternoon) for IOP1 and IOP2 | Regardless of cloud cover (clear vs non-clear days) |
| Time of Day (morning vs. afternoon) for clear vs. non-clear days | Regardless of IOP1 and IOP2 |
| Time of Day (morning vs. afternoon) for clear vs. non-clear days during IOP1 and IOP2 | |

367

368

369 4. Results

370 As noted previously, this paper aims to provide additional understanding of the impacts
371 of irrigation on L-A interactions and the convective environment. Hence, an analyses of coupling
372 metrics were completed for IOP1 and IOP2 (section 3.1) to determine whether periods of
373 growing season alone can play an important role, regardless of time of day (morning vs.
374 afternoon) and sky condition (clear versus cloudy condition) (Table 2). Note that typically
375 afternoons are more favorable for convection development while during clear-skies irrigation can
376 play an important role in L-A interactions (e.g., Rappin et al. 2021, 2022). Also, cloudy days
377 could be linked to large-scale synoptic activities, which may dampen or mask L-A interactions.
378 Furthermore, IOP1 and IOP2 represent the early and peak growing season, respectively and
379 during IOP2 irrigation becomes widespread.

380 Subsequently, an analysis of coupling metrics by clear versus cloudy days, regardless of
381 IOP1 and IOP2, was used to determine whether irrigation forcing is sufficiently strong such that
382 growing period did not matter. Then the three metrics were analyzed by clear versus cloudy days
383 for IOP1 and IOP2 to determine whether growing periods along with background conditions
384 provides an improved ‘signal’ of land use forcing (regardless of time of day) on L-A interactions
385 and the convective environment. It is expected that clear days during IOP2 would provide the
386 most noticeable response of the atmosphere to irrigation.

387 Coupling metrics subset by time of day (morning versus afternoon, regardless of IOP1 or
388 IOP2); by time of day and IOP1 and IOP2; by time of day and clear versus cloudy conditions
389 (regardless of IOP1 and IOP2); and by time of day, IOP1 and IOP2, and clear and cloudy
390 conditions were also analyzed.

391

392 *a. Early (IOP1) and Peak (IOP2) Growing Season*

393 Table 3 shows the mean statistics for CTP, HI_{low} , and LCL Deficit for IOP1 and IOP2
394 and by clear and non-clear days. Differences in CTP and HI_{low} during IOP1 for irrigated and
395 non-irrigated land use were not statistically significant. However, differences in LCL Deficit for
396 these two land uses were statistically significant ($p < 0.05$). Average LCL deficits were the

397 lowest (287.70 m) for the non-irrigated ISS2 site (Table 3). Additionally, the difference between
398 the average values of LCL Deficit among ISS2 and all other sites is very large (up to 264 m).

399 During IOP2, differences in HI_{low} between irrigated and non-irrigated land use were not
400 statistically significant. Average HI_{low} was the highest (lowest) for the non-irrigated ISS2
401 (irrigated ISS3) site at 11.41 K (14.79 K) (differences are statistically significant; $p < 0.05$). In
402 other words, average HI_{low} for non-irrigated ISS2 was 0.29 to 3.38 K higher than the other sites
403 (Table 3). Irrigated ISS3 (35.49 m) and DOW8 (60.70 m) show the two lowest LCL Deficit
404 values while non-irrigated ISS2 shows the highest (101.44 m). During IOP2, all sites
405 demonstrate lower LCL Deficit and HI_{low} values compared to IOP1. Irrigated ISS3 and irrigated
406 DOW8 depict the largest decline forced by irrigation. Overall, irrigated ISS3 and DOW8 depict
407 more favorable conditions for convection compared to the non-irrigated areas, regardless of clear
408 and non-clear conditions (benign vs non-benign, Frye and Mote 2010) and time of day.

409
410
411
412
413
414
415
416
417
418
419
420
421
422
423
424
425
426

427 Table 3. Mean CTP, HI_{low} , and LCL Deficit (LCL-PBL) for IOP1, IOP2, clear days, and non-
 428 clear days. Statistical significance tests for the differences in means are completed for *Irrigated*
 429 *ISS3 vs Non-irrigated ISS2, Irrigated DOW8 vs non-irrigated ISS2, Irrigated ISS3 vs*
 430 *Transitional DOW6*. For brevity, significance tests were not completed for all possible
 431 combinations (e.g., ISS3 vs DOW7). Bold and italicized variables represent those which have a p
 432 < 0.05 for statistical significance test.

433

434

| IOP 1 | | | |
|------------------|--------------------------|------------------------------------|-------------------------------|
| Site Name | CTP (J/kg) | HI_{low} (K) | <i>LCL Deficit (m)</i> |
| ISS2 | 115.27 | 20.77 | <i>287.70</i> |
| ISS3 | 122.25 | 21.32 | <i>417.13</i> |
| DOW6 | 115.72 | 20.66 | <i>521.61</i> |
| DOW7 | 109.05 | 20.77 | 551.42 |
| DOW8 | 110.25 | 20.89 | <i>468.15</i> |
| IOP 2 | | | |
| Site Name | CTP (J/kg) | <i>HI_{low} (K)</i> | LCL Deficit (m) |
| ISS2 | 76.78 | <i>14.79</i> | 101.44 |
| ISS3 | 96.94 | <i>11.41</i> | 35.49 |
| DOW6 | 75.52 | <i>14.18</i> | 102.05 |
| DOW7 | 70.86 | 14.50 | 63.66 |
| DOW8 | 68.65 | <i>13.18</i> | 60.70 |
| Clear | | | |
| Site Name | <i>CTP (J/kg)</i> | <i>HI_{low} (K)</i> | <i>LCL Deficit (m)</i> |
| ISS2 | <i>50.34</i> | <i>22.82</i> | <i>203.93</i> |
| ISS3 | <i>106.27</i> | <i>19.63</i> | <i>290.48</i> |
| DOW6 | <i>67.97</i> | <i>21.70</i> | <i>405.87</i> |
| DOW7 | 70.17 | 21.97 | 427.19 |
| DOW8 | <i>73.21</i> | <i>20.10</i> | <i>312.60</i> |
| Non-Clear | | | |
| Site Name | CTP (J/kg) | HI_{low} (K) | LCL Deficit (m) |
| ISS2 | 115.61 | 15.62 | 191.63 |
| ISS3 | 111.02 | 14.97 | 199.47 |
| DOW6 | 108.82 | 15.56 | 271.45 |
| DOW7 | 99.68 | 15.77 | 255.82 |
| DOW8 | 97.62 | 15.77 | 245.18 |

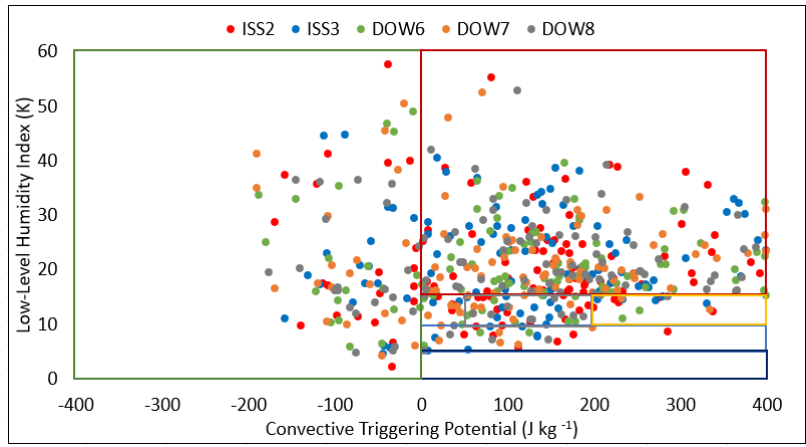
444

445

446

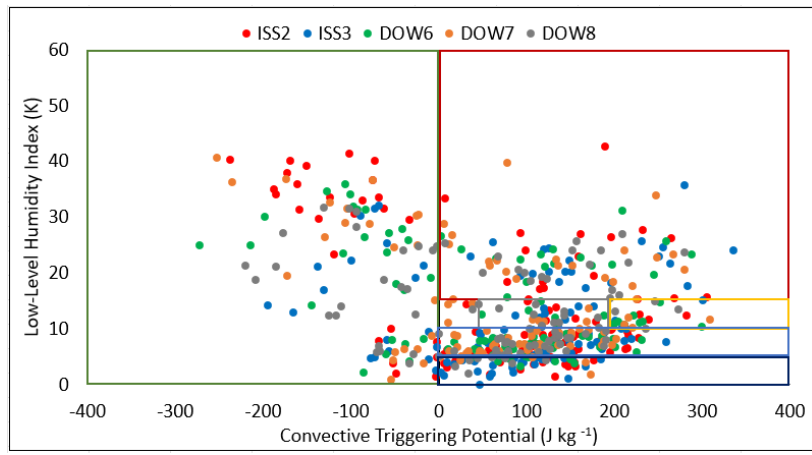
447

448 a)



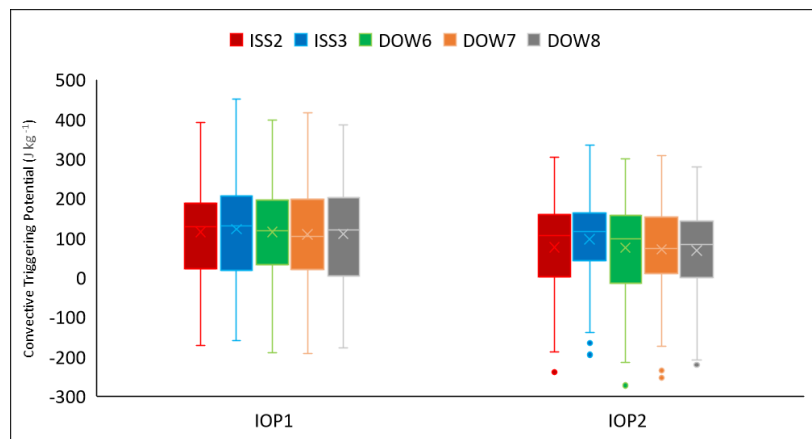
449

450 b)



451

452 c)

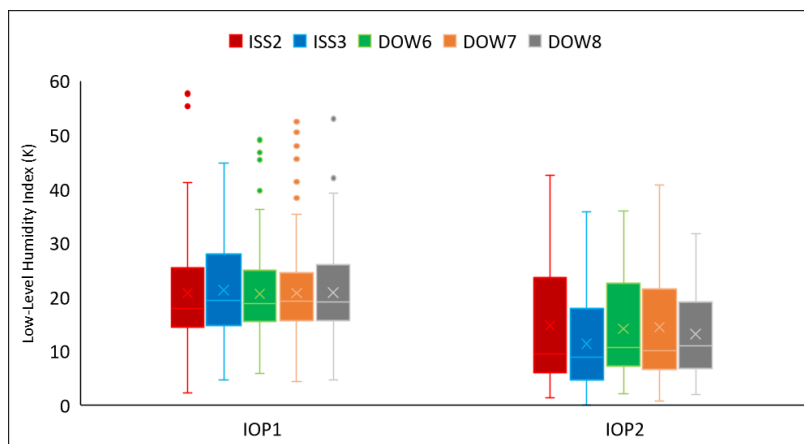


453

454

455

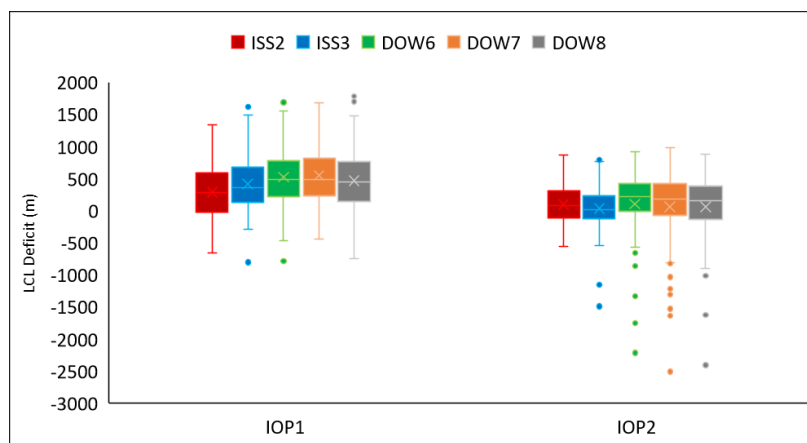
456 d)



457

458

459 e)



460

461

462 Figure 3a-e: Distributions of coupling metrics using: a) scatter plots of CTP and HI_{low} for IOP1,

463 and b) IOP2; box and whisker plots of c) CTP, d) HI_{low} , and e) LCL Deficit for IOP1

464 and IOP2. Dots and boxes with different colors represent radiosonde launching sites, which are

465 identified at the top of each panel. ISS3 and DOW8 are *irrigated* locations, ISS2 and DOW7 are

466 *non-irrigated*, and DOW6 is a *transitional* land use zone (from irrigated to non-irrigated).

467 Figure 3a-b shows the scatter plots of CTP and HI_{low} along with colored boxes depicting

468 categories identified in Table 1 and Figure 2. Most observations, regardless of location, were

469 concentrated in the too dry for precipitation range ($CTP > 0$ and $HI_{low} \geq 15$) during IOP1 (Figure

470 3a). However, during IOP2, most observations were concentrated in the wet soil advantage (CTP

471 > 0 and $10 < HI_{low} < 15$). This change in the distribution of observations reflects the change in
472 the land-surface conditions from IOP 1 to IOP2. Given the lack of irrigation during the early
473 growing season (IOP1) and widespread irrigation during the peak growing season (IOP2), these
474 results imply that irrigation is playing an important role in modifying the convective
475 environment.

476 Figure 3c-e shows the box and whisker plots of CTP, HI_{low} , and LCL Deficit,
477 respectively. The median CTP value for irrigated ISS3 during IOP2 was higher than the other
478 sites. HI_{low} and LCL Deficits show a noticeable lowering of their median values for irrigated
479 ISS3 during IOP2, indicating the influence of irrigation. This result also suggests a moistening of
480 the lower atmosphere linked to irrigated land use (Rappin et al. 2021, 2022; Phillips et al. 2022).

481

482 *b. Clear and Non-Clear Days*

483 During clear days, average CTP was the highest (lowest) over irrigated ISS3 (non-
484 irrigated ISS2) at 106.27 J kg^{-1} (50.34 J kg^{-1}) (Table 3). In other words, average CTP for irrigated
485 ISS3 was $33.06\text{-}55.93 \text{ J kg}^{-1}$ higher than the other sites. Average HI_{low} was the lowest (highest)
486 over irrigated ISS3 (non-irrigated ISS2) at 19.62 K (22.82 K). Thus, average HI_{low} over irrigated
487 ISS3 was $0.43\text{-}3.2 \text{ K}$ lower compared to the other sites (Table 3). Average LCL Deficits were the
488 lowest (highest) over the non-irrigated ISS2 (DOW7) site at 203.93 m (427.19 m). Hence,
489 average LCL Deficits at ISS2 are 86.55 to 223.36 m lower compared to the other sites (Table 3).

490 Although differences in CTP, HI_{low} , and LCL Deficit between irrigated and non-irrigated
491 sites for non-clear days were not statistically significant, we found an average increase of CTP
492 and lowering of HI_{low} and LCL Deficit values for all sites. Based on the observations, it is
493 difficult to discern the influence of the land surface simply based on the large-scale atmospheric
494 set-up. In other words, it is important to conduct an analysis that also incorporates land-surface
495 conditions such as early (IOP1) versus peak (IOP2) growing season which captures the extent of
496 the crop/vegetation cover and status of irrigation/soil moisture.

497

498

499

500 *c. Clear and Non-clear days during Early (IOP1) and Peak (IOP2) Growing Season*

501 To further understand irrigation impacts, an analysis using coupling metrics for clear and
502 non-clear days over IOP1 and IOP2 was completed. Table 4 shows the mean values of CTP,
503 HI_{low} , and LCL Deficit along with the results of the statistical significance testing. During clear
504 days in IOP1, differences in CTP between irrigated and non-irrigated land use were statistically
505 not significant. Average HI_{low} during clear days in IOP1 was the highest (lowest) for the irrigated
506 ISS3 (non-irrigated ISS2) site at 19.61 K (16.54 K). In other words, irrigated ISS3 has average
507 HI_{low} values that are 0.77 to 3.07 K higher than the other sites (Table 4). Average LCL Deficits
508 during clear days in IOP1 were the highest (lowest) for the non-irrigated DOW7 (non-irrigated
509 ISS2) site at 435.98 m (157.44 m). Average LCL Deficits for the non-irrigated DOW7 site are
510 8.7 to 287.24 m higher than the other sites (Table 4). Overall, based on LCL Deficit and HI_{low} the
511 non-irrigated land shows slightly more favorability towards convective development.

512 During clear days in IOP2, average CTP was the highest (lowest) for the irrigated ISS3
513 (non-irrigated ISS2) site at 76.99 J kg⁻¹ (-28.75 J kg⁻¹). Moreover, CTP at ISS3 during IOP2 was
514 55.09 to 105.74 J kg⁻¹ higher than the other sites (Table 4). Average HI_{low} was the highest
515 (lowest) for the non-irrigated ISS2 (irrigated ISS3) site at 30.68 K (19.66 K). Average LCL
516 Deficit was the highest (lowest) for the non-irrigated DOW7 (irrigated ISS3) site at 405.96 m
517 (180.46 m) and was 36.66 to 225.5 m higher compared to the other sites (Table 4). These results
518 suggest that, compared to non-irrigated land use, irrigated land use increased convective
519 potential during IOP2 when irrigation applications increased due to increases in crop water
520 demand.

521 Average LCL Deficits during non-clear days in IOP1 were the lowest for DOW7, a non-
522 irrigated site, at 607.26 m and were 40.86 to 251.41 m higher than the other sites (Table 4). For
523 IOP2 this condition reversed for DOW7 which showed the lowest average LCL Deficit.
524 However, if we consider results from CTP, HI_{low} , and LCL Deficit (differences are not
525 statistically significant) for the two most well-representative irrigated (ISS3) and non-irrigated
526 (ISS2) sites then during non-clear days in IOP2 conditions were comparatively more favorable
527 for convection development over irrigated land use. In short, if land use forcing is sufficiently
528 large, it does not matter whether background atmospheric conditions are ‘benign’ or ‘non-
529 benign’ (e.g., Frye and Mote 2010), it’s impacts on the convective environment are discernable.

530

531 Table 4. Mean CTP, HI_{low} , and the LCL deficit (LCL-PBL) for clear and non-clear days during
 532 IOP1 and IOP2. Statistical significance tests for the differences in means are completed for
 533 *Irrigated ISS3 vs Non-irrigated ISS2, Irrigated DOW8 vs ISS2, Irrigated ISS3 vs Transitional DOW6.*
 534 For brevity, significance tests were not completed for all possible combinations (e.g., ISS3 vs
 535 DOW7). Bold values represent those which have a $p < 0.1$ in t -tests, while bold and italicized
 536 values represent those which have a $p < 0.05$.

| Clear IOP 1 | | | |
|----------------|----------------------|---------------------|----------------------|
| Site Name | CTP (J/kg) | HI_{low} (K) | LCL Deficit (m) |
| ISS2 | 113.61 | <i>16.54</i> | <i>157.44</i> |
| ISS3 | 129.69 | <i>19.61</i> | <i>381.09</i> |
| DOW6 | 119.01 | <i>18.30</i> | <i>435.98</i> |
| DOW7 | 108.78 | <i>18.11</i> | 444.68 |
| DOW8 | 117.98 | <i>18.84</i> | <i>325.43</i> |
| Clear IOP 2 | | | |
| Site Name | CTP (J/kg) | HI_{low} (K) | LCL Deficit (m) |
| ISS2 | <i>-28.75</i> | <i>30.68</i> | <i>260.39</i> |
| ISS3 | <i>76.99</i> | <i>19.66</i> | <i>180.46</i> |
| DOW6 | <i>5.98</i> | <i>25.83</i> | <i>369.3</i> |
| DOW7 | <i>21.90</i> | <i>26.79</i> | 405.96 |
| DOW8 | <i>17.24</i> | <i>21.69</i> | <i>297.01</i> |
| Non-Clear IOP1 | | | |
| Site Name | CTP (J/kg) | HI_{low} (K) | LCL Deficit (m) |
| ISS2 | 116.11 | 22.89 | <i>355.85</i> |
| ISS3 | 118.53 | 22.18 | <i>435.98</i> |
| DOW6 | 114.05 | 21.86 | <i>566.4</i> |
| DOW7 | 109.19 | 22.14 | 607.26 |
| DOW8 | 106.27 | 21.95 | <i>542.81</i> |
| Non-Clear IOP2 | | | |
| Site Name | CTP (J/kg) | HI_{low} (K) | LCL Deficit (m) |
| ISS2 | 115.16 | 9.02 | 36.94 |
| ISS3 | 104.20 | 8.41 | -23.33 |
| DOW6 | 103.74 | 9.45 | -6.39 |
| DOW7 | 90.45 | 9.59 | -75.24 |
| DOW8 | 89.22 | 9.77 | -35.2 |

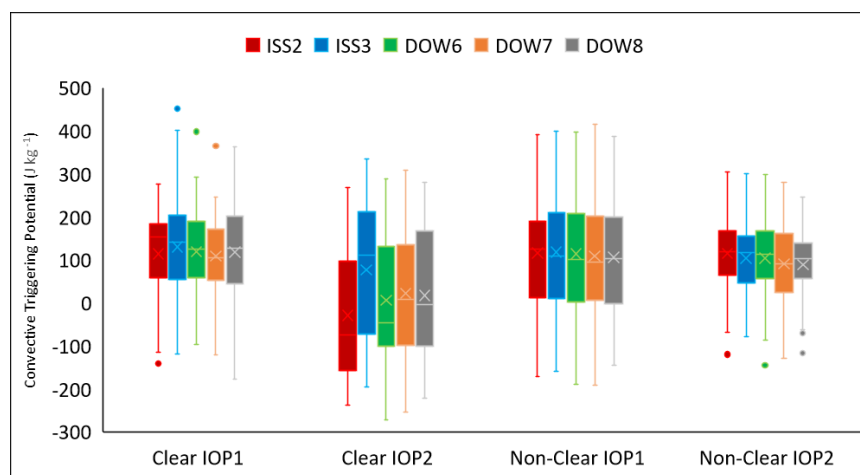
557 Figure 4a-c shows the box and whisker plots of CTP, HI_{low} , and LCL Deficits for all sites
 558 by cloud cover and IOP. For clear days in IOP1, median values of CTP were the highest (slightly
 559 $< 200 \text{ J kg}^{-1}$) for the non-irrigated ISS2 location (Figure 4a). Median values of HI_{low} were the
 560 lowest ($10 < HI_{low} < 15$) for the non-irrigated ISS2 site. Together they indicate a transition zone
 561 (Table 1) for convection, which is expected for non-irrigated land use during IOP1 when the land

562 surface was sufficiently and naturally wet (to support the rainfed crop) in the eastern part of the
 563 study area (Figure 4b). Median values of LCL Deficits during clear days in IOP1 were the
 564 highest (lowest) for the transitional land use DOW6 (non-irrigated ISS2) site. Negative skewness
 565 was noted for the transitional land use DOW6 and irrigated DOW8 sites. In other words, above
 566 average values of LCL Deficit appeared more frequently at these sites (Figure 4c).

567 For clear days in IOP2, median values for CTP were the highest (lowest) for the irrigated
 568 ISS3 (non-irrigated ISS2) site (Figure 4a). Negative skew was noticed for the non-irrigated ISS2,
 569 irrigated ISS3, and irrigated DOW8 sites (Figure 3a). Median values of HI_{low} during clear days in
 570 IOP2 were the lowest (~19 K) (highest; ~30 K) for the irrigated ISS3 (non-irrigated ISS2) site
 571 (Figure 4b). Median values of LCL Deficits were the lowest for the irrigated ISS3 site. (Figure
 572 4c). Together these metrics demonstrate that irrigated land use favorably impacted the
 573 convective environment on clear days. These changes are most visible for ISS3 (irrigated land
 574 use) and ISS2 (non-irrigated land use).

575

576 a)



577

578

579

580

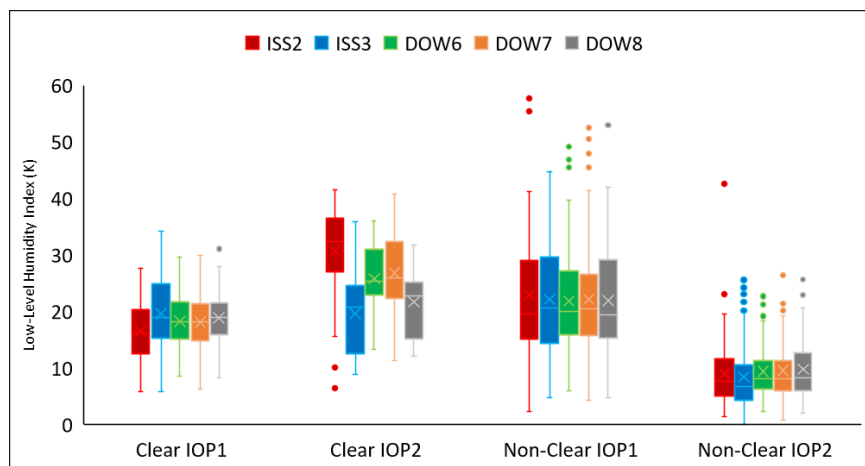
581

582

583

584

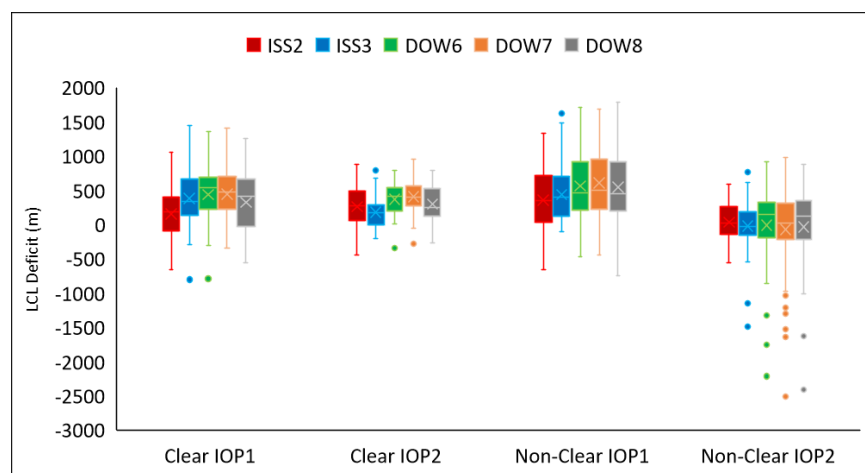
585 b)



586

587

588 c)



589

590 Figure 4a-c: Box and whisker plots of: a) CTP, b) HI_{low} , and c) LCL deficit by cloud cover and
591 IOP. Boxes with different colors represent different radiosonde launching sites, which are
592 identified at the top of each panel. ISS3 and DOW8 are *irrigated* locations, ISS2 and DOW7 are
593 *non-irrigated*, and DOW6 is a *transitional* land use zone (from irrigated to non-irrigated).

594

595 For non-clear days in IOP1, the median value of CTP was the highest (lowest) for the
596 non-irrigated ISS2 (non-irrigated DOW7) site. A slight positive skew was noted for irrigated
597 ISS3, transitional land use DOW6, and non-irrigated DOW7 sites (Figure 4a). Median values of
598 HI_{low} were the highest (lowest) for the irrigated ISS3 (non-irrigated ISS2) site (Figure 4b).
599 Median values of LCL Deficit during non-clear days in IOP1 were the highest (lowest) for the

600 non-irrigated DOW7 (non-irrigated ISS2) site (Figure 4c). For non-clear days in IOP2, median
 601 values of CTP were the highest (lowest) for the irrigated ISS3 (non-irrigated DOW7) site. The
 602 lowest median values of HI_{low} and LCL Deficit values were found for irrigated ISS3. There was
 603 a clear shift towards lower HI_{low} and LCL Deficit values during IOP2 under non-clear days
 604 across all sites with the most noticeable changes over irrigated land use (ISS3) (Table 4). Again,
 605 these suggest irrigation forcing on the convective environment.

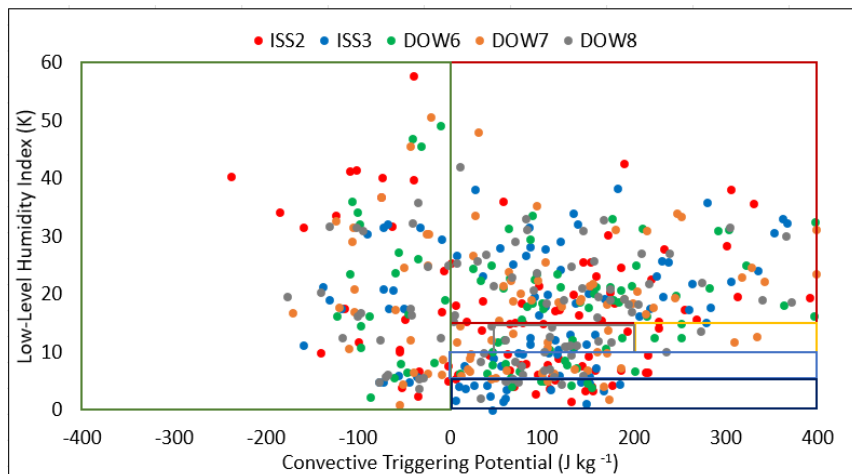
606

607 *d. Time of Day (morning vs afternoon)*

608 CTP, HI_{low} , and LCL Deficit were calculated by time of day to investigate whether time
 609 of day has an influence on L-A coupling. First, we analyzed the data based on time of day
 610 *without* considering land use and period of the season [early growing season (IOP1) vs. peak
 611 growing season (IOP2)] (Figure 5a-e). As noted previously, soundings launched from 1300 UTC
 612 to 1700 UTC were considered morning soundings while soundings launched from 1900 UTC to
 613 0100 UTC were afternoon soundings. Figure 5a-e shows the distributions of coupling metrics by
 614 time of day, with Figure 5a-b showing the scatter plots of CTP and HI_{low} for morning and
 615 afternoon and Figure 5c-e showing the box and whisker plots of CTP, HI_{low} , and LCL Deficits.
 616 For both mornings and afternoons, overall differences in CTP, HI_{low} , and LCL Deficit were not
 617 statistically significant. However, the distribution for the morning is more scattered while the
 618 afternoon data are concentrated at higher values signifying more mixing in the boundary layer
 619 atmosphere.

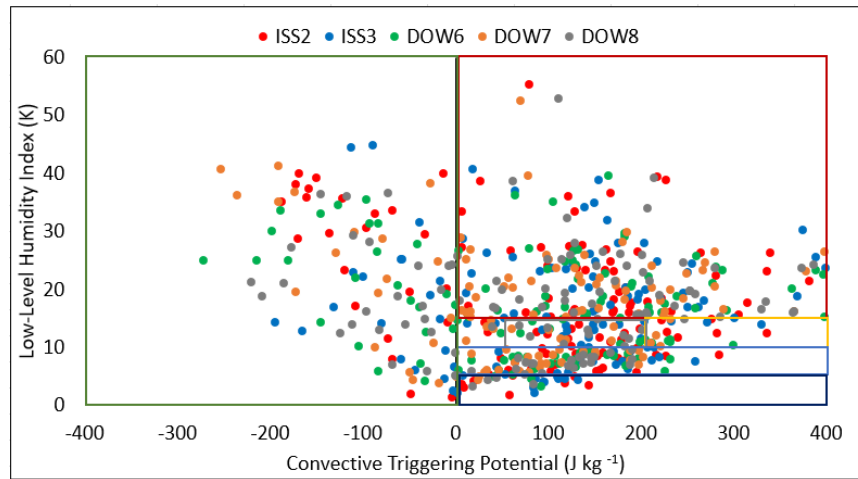
620

621 a)



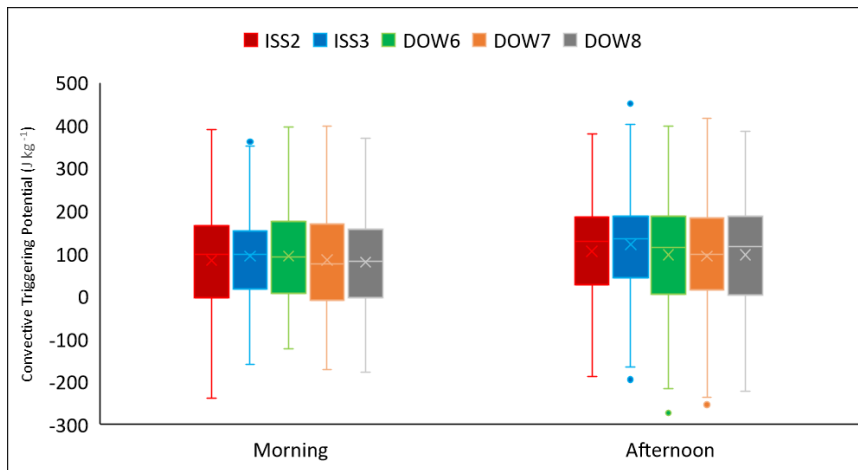
622

623 b)



624

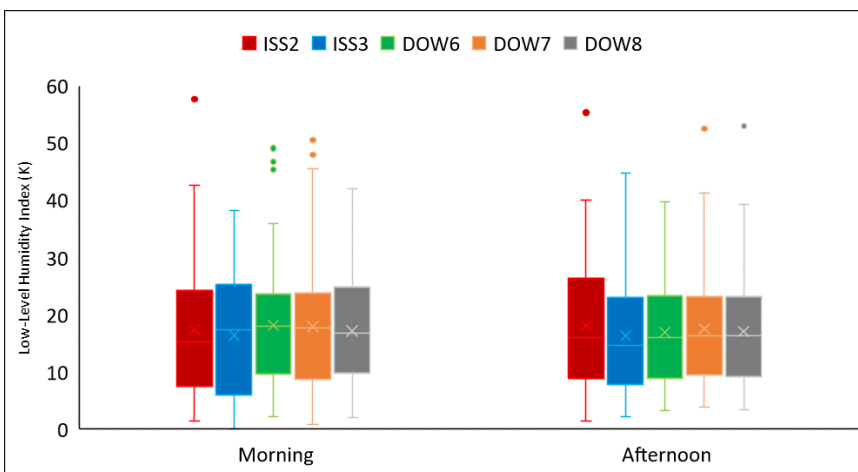
625 c)



626

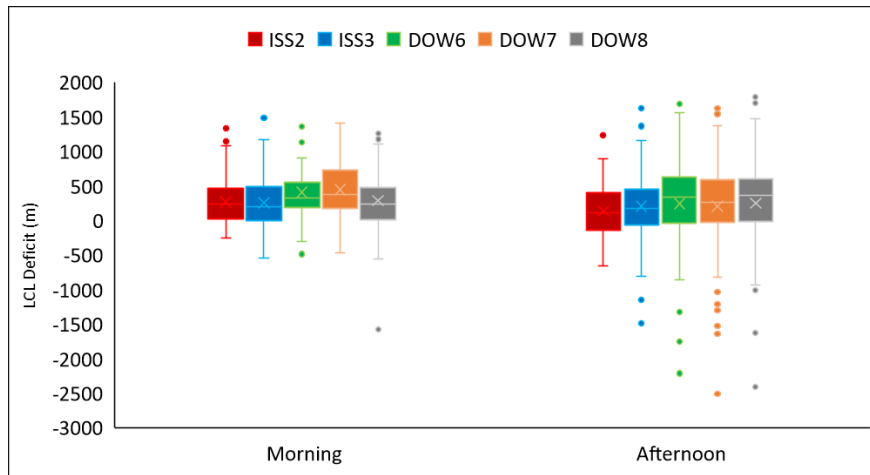
627

628 d)



629

630 e)



631

632

633

634 Figure 5a-c: Scatter plots of CTP and HI_{low} for: a) morning and b) afternoon; and c-e) box
635 and whisker plots of CTP, HI_{low} , and LCL Deficit. Dots and boxes with different colors represent
636 radiosonde launching sites, which are identified at the top of each panel. ISS3 and DOW8 are
637 irrigated locations, ISS2 and DOW7 are non-irrigated, and DOW6 is a transitional land use
638 zone (from irrigated to non-irrigated).

639

640 e. Time of Day and Early IOP1 and Peak (IOP2) Growing Season

641 To further understand L-A interactions, the coupling metrics were analyzed by time of
642 day and IOP1 and IOP2. Table 4 shows the mean values of CTP, HI_{low} , and LCL Deficit. For
643 mornings in IOP1, differences in CTP and HI_{low} for irrigated and non-irrigated land use were
644 statistically not significant. However, differences in LCL Deficit between irrigated and non-
645 irrigated land use were statistically significant ($p < 0.05$) (Table 5). Average LCL Deficits during
646 the mornings of IOP1 were the highest (lowest) for the non-irrigated DOW7 (non-irrigated ISS2)
647 site at 617.78 m (393.41 m). In other words, DOW7 had average LCL Deficits that are 45.32 to
648 224.37 m higher than the other sites (Table 4). Due to drier condition and hence more sensible
649 heat flux over non-irrigated DOW7, both PBL and LCL heights increase and resulted in higher
650 LCL Deficits (*cf.*, Figure 10, Rappin et al. 2021).

651 For mornings in IOP2, differences in CTP between the two land uses were not
652 statistically significant. Average HI_{low} during mornings in IOP2 was the highest (lowest) for the
653 transitional land use DOW6 (irrigated ISS3) site at 14.77 K (11.64 K) (Table 5). The lowest

654 HI_{low} value is linked to the irrigated ISS3 while the highest with the transitional land use DOW6
655 location, suggesting impacts of land use and surface moistness. The differences in HI_{low} between
656 irrigated ISS3 and transitional land use DOW6 were statistically significant ($p < 0.1$). Average
657 LCL Deficits during mornings of IOP2 were the highest (lowest) for the non-irrigated DOW7
658 (irrigated ISS3) site at 262.46 m (68.60 m). In other words, average LCL Deficits for the non-
659 irrigated DOW7 site were 32.76 to 193.86 m higher than all other sites. Also, the second lowest
660 LCL Deficit value (85.18 m) was observed for irrigated DOW8. The differences in LCL Deficits
661 between irrigated and non-irrigated land use were statistically significant ($p < 0.1$). These low
662 LCL Deficit and HI_{low} coupling metrics are an indication of irrigation's impact.

663 For afternoons in IOP1, differences in CTP, HI_{low} , and LCL Deficit between irrigated and
664 non-irrigated locations were not statistically significant. The same applies for CTP and LCL
665 Deficit in IOP2, while HI_{low} shows a statistically significant difference ($p < 0.05$) (Table 5).
666 Further, LCL Deficit is noticeably lower during afternoons of IOP2 for all locations and
667 compared to the mornings of IOP1 and IOP2. Additionally, during IOP2 CTP and HI_{low} were
668 indicating a wet soil advantage for irrigated ISS3 and irrigated DOW8 locations. It is observed
669 that, compared to IOP1 HI_{low} (> 20 K), IOP2 HI_{low} was lower (11.23-14.84 K) during the
670 afternoons. Overall, it was found that convective favorability increased for all sites during IOP2,
671 with irrigated land use providing higher favorability, regardless of cloud conditions (clear or
672 non-clear) (Table 5).

673
674
675
676
677
678
679
680
681
682
683

684 Table 5: Mean CTP, HI_{low} , and the LCL Deficit (LCL-PBL) for morning and afternoon of IOP1
 685 and IOP2. Statistical significance tests for the differences in means are completed for *Irrigated*
 686 ISS3 vs *Non-irrigated* ISS2, *Irrigated* DOW8 vs ISS2, *Irrigated* ISS3 vs *Transitional* DOW6. For
 687 brevity, significance tests were not completed for all possible combinations (e.g., ISS3 vs
 688 DOW7). Bold values represent those which have a $p < 0.1$ in t -tests, while bold and italicized
 689 represent those which have a $p < 0.05$.

690

| Morning IOP 1 | | | |
|-----------------------|------------|----------------|-----------------|
| Site Name | CTP (J/kg) | HI_{low} (K) | LCL Deficit (m) |
| ISS2 | 95.19 | 20.07 | 393.41 |
| ISS3 | 101.45 | 21.22 | 439.25 |
| DOW6 | 115.30 | 21.41 | 572.46 |
| DOW7 | 102.25 | 21.16 | 617.78 |
| DOW8 | 91.00 | 20.48 | 484.78 |
| Morning IOP 2 | | | |
| Site Name | CTP (J/kg) | HI_{low} (K) | LCL Deficit (m) |
| ISS2 | 72.62 | 14.73 | 142.00 |
| ISS3 | 86.31 | 11.64 | 68.60 |
| DOW6 | 72.36 | 14.77 | 229.70 |
| DOW7 | 66.22 | 14.49 | 262.46 |
| DOW8 | 67.83 | 13.66 | 85.18 |
| Afternoon IOP1 | | | |
| Site Name | CTP (J/kg) | HI_{low} (K) | LCL Deficit (m) |
| ISS2 | 130.34 | 21.29 | 203.15 |
| ISS3 | 137.85 | 21.40 | 399.44 |
| DOW6 | 116.05 | 20.09 | 480.93 |
| DOW7 | 114.32 | 20.47 | 498.34 |
| DOW8 | 125.18 | 21.21 | 454.85 |
| Afternoon IOP2 | | | |
| Site Name | CTP (J/kg) | HI_{low} (K) | LCL Deficit (m) |
| ISS2 | 79.91 | 14.84 | 70.47 |
| ISS3 | 104.91 | 11.23 | 10.22 |
| DOW6 | 77.93 | 13.72 | 4.58 |
| DOW7 | 74.34 | 14.51 | -88.16 |
| DOW8 | 69.27 | 12.81 | 41.99 |

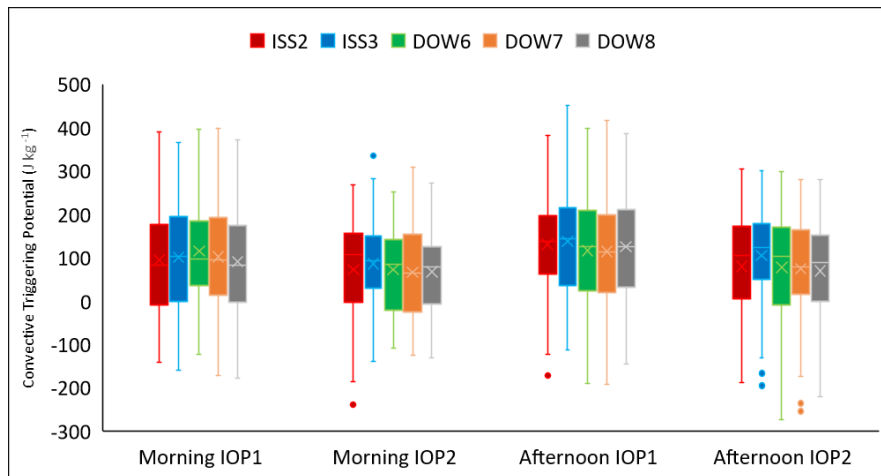
691

692 Figure 6a-c shows the box and whisker plots of CTP, HI_{low} , and LCL Deficit by time of
 693 day and IOP. Based on the LCL Deficit and HI_{low} values, it is evident that afternoons of IOP2
 694 were more favorable for convection development and agrees with the previous assessment linked
 695 to Table 5.

696

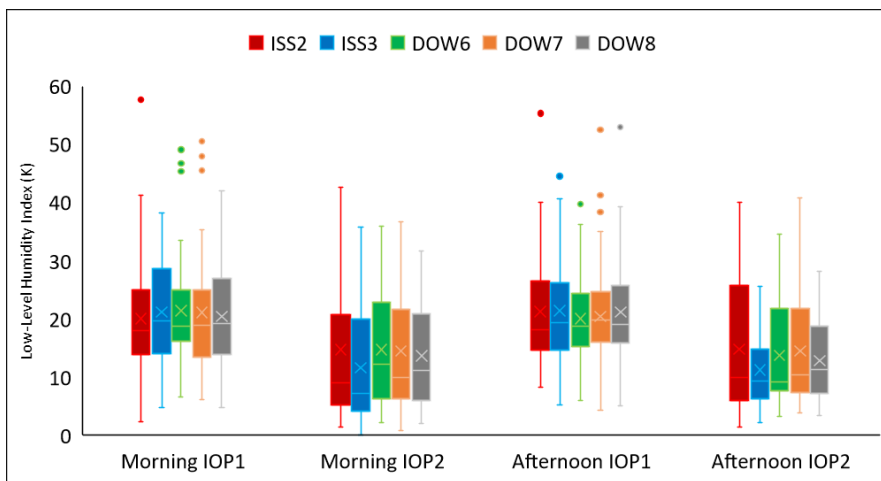
697

698 a)



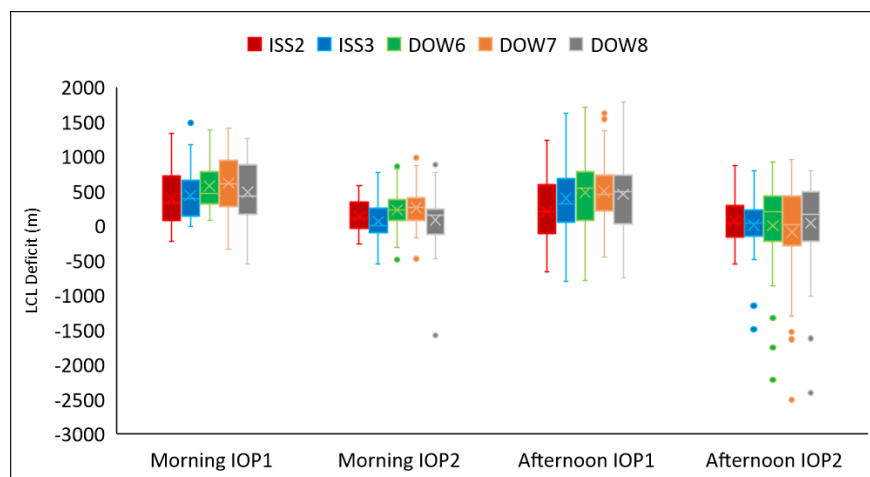
699

700 b)



701

702 c)



703

704

705 Figure 6: Box and whisker plots of: a) CTP, b) HI_{low} , and c) LCL Deficit by time of day and
706 IOP. Boxes with different colors represent radiosonde launching sites, which are identified at the
707 top of each panel. ISS3 and DOW8 are *irrigated* locations, ISS2 and DOW7 are *non-irrigated*,
708 and DOW6 is a *transitional* land use zone (from irrigated to non-irrigated).

709

710 *f. Time of Day and Cloud Cover (clear vs non-clear day)*

711 Table 5 shows the average values of CTP, HI_{low} , and LCL Deficit regardless of IOPs.
712 For clear mornings, the average CTP was the highest (lowest) for irrigated ISS3 (non-irrigated
713 ISS2) site at 71.41 J kg^{-1} (16.77 J kg^{-1}) (Table 6). The highest (lowest) HI_{low} value was 21 K
714 (19.60 K) for transitional land use DOW6 (irrigated DOW8). The largest (lowest) LCL Deficit
715 was 430.48 m (242.32 m) for transitional land use DOW6 (irrigated DOW8). DOW8 was located
716 over an irrigated area and coupling metrics indicate the influence of irrigated land use.
717 Differences in HI_{low} and LCL Deficits for irrigated and non-irrigated land use during clear
718 mornings were statistically not significant.

719 Average CTP during clear afternoons is the highest (lowest) for the irrigated ISS3 (non-
720 irrigated ISS2) site at 132.40 J kg^{-1} (75.51 J kg^{-1}) (Supplementary Table 1). In addition, average
721 HI_{low} during clear afternoons is the highest (lowest) for the non-irrigated ISS2 (irrigated ISS3)
722 site at 24.43 K (19.39 K) (Supplementary Table 1). The difference of CTP and HI_{low} values
723 between irrigated and non-irrigated land use and clear afternoons is statistically significant ($p <$
724 0.05). For non-clear mornings, differences in CTP and HI_{low} over the two land uses were not
725 statistically significant. For non-clear mornings, the average LCL Deficit was the highest
726 (lowest) for the non-irrigated DOW7 (irrigated ISS3) site at 451.65 m (234.38 m). Based on the
727 CTP, HI_{low} , and LCL Deficit, and compared to non-clear mornings, it appears that non-clear
728 afternoons are more favorable for convective development for all land use types during
729 GRAINEX (Supplementary Table 1).

730

731

732

733

734

735

736 Supplementary Figure 1a-c shows the box and whisker plots of CTP, HI_{low} , and LCL
737 Deficits by cloud cover and time of day. Again, compared to clear mornings, CTP values tend to
738 be higher during clear afternoons. Irrigated ISS3 shows the most noticeable CTP and HI_{low}
739 changes from morning to afternoon. For clear mornings, median values of CTP were the highest
740 (lowest) for the ISS3 (ISS2) site.

741

742 *g. Time of Day and Cloud Cover during Early (IOP1) and Peak (IOP2) Growing Season*

743 To further understand the influence of irrigation and land use, we assessed coupling
744 metrics for clear mornings of IOP1 and IOP2, clear afternoons of IOP1 and IOP2, non-clear
745 mornings of IOP1 and IOP2, and non-clear afternoons of IOP1 and IOP2. On clear days when
746 land use forcing is expected to be higher, it is found that LCL Deficit was the lowest (182.5 m)
747 in the afternoon over irrigated areas (ISS3) during IOP2 (Table 6). It is also found that CTP
748 (66.42 J kg^{-1}) and HI_{low} (17.58 K) were the highest and the lowest, respectively, over irrigated
749 land use (ISS3) compared to the other locations in the afternoon during IOP2 (Table 6). The
750 difference between irrigated and non-irrigated land use for CTP and HI_{low} was statistically
751 significant. Similar results were found during IOP2 clear mornings, however, the difference
752 between irrigated and non-irrigated land use is not statistically significant. These results are
753 further shown in Figure 7a-c.

754 For non-clear days of IOP1 and IOP2 when larger-scale influences were prominent, land
755 use influence on the atmosphere and its convective environment was not as clear. However, both
756 the afternoon and mornings of IOP2 show clearer land use influence via lower HI_{low} and LCL
757 Deficit and relatively higher CTP. Further assessment shows that the second lowest HI_{low} and the
758 second highest CTP during the afternoon hours of IOP2 occurred over irrigated areas, coincident
759 with negative LCL Deficit, suggesting favorable conditions for cloud development. Hence,
760 irrigation impacts are discernable even when the large-scale atmospheric influence is present.

761

762

763

764

765

766

767 Table 6: Mean CTP, HI_{low}, and LCL Deficit (LCL-PBL) for clear morning of IOP1 and IOP2,
768 clear afternoon of IOP1 and IOP2, non-clear morning of IOP1 and IOP2, and non-clear afternoon
769 of IOP1 and IOP2. Statistical significance tests for the differences in means are completed for
770 *Irrigated ISS3 vs Non-irrigated ISS2, Irrigated DOW8 vs ISS2, Irrigated ISS3 vs Transitional DOW6.*
771 For brevity, significance tests were not completed for all possible combinations (e.g., ISS3 vs
772 DOW7). Bold values represent those which have a $p \leq 0.1$ in t-tests, while bold and italicized
773 represent those which have a $p \leq 0.05$.

774

| Clear Morning IOP1 | | | | Clear Morning IOP2 | | | |
|--------------------------|------------|-----------------------|------------------------|--------------------------|---------------|-----------------------|-----------------|
| Site Name | CTP (J/kg) | HI _{low} (K) | LCL Deficit (m) | Site Name | CTP (J/kg) | HI _{low} (K) | LCL Deficit (m) |
| ISS2 | 54.33 | 13.94 | 284.71 | ISS2 | -30.18 | 29.10 | 254.33 |
| ISS3 | 55.69 | 17.96 | 429.43 | ISS3 | 91.07 | 22.43 | 177.75 |
| DOW6 | 55.26 | 16.49 | 509.46 | DOW6 | 21.57 | 26.27 | 338.34 |
| DOW7 | 48.75 | 15.25 | 458.92 | DOW7 | 23.80 | 27.23 | 390.13 |
| DOW8 | 47.42 | 16.75 | 325.27 | DOW8 | 38.67 | 23.17 | 145.53 |
| Clear Afternoon IOP1 | | | | Clear Afternoon IOP2 | | | |
| Site Name | CTP (J/kg) | HI _{low} (K) | LCL Deficit (m) | Site Name | CTP (J/kg) | HI _{low} (K) | LCL Deficit (m) |
| ISS2 | 158.06 | 18.48 | 68.35 | ISS2 | -27.68 | 31.86 | 264.94 |
| ISS3 | 185.19 | 20.84 | 347.25 | ISS3 | 66.42 | 17.58 | 182.5 |
| DOW6 | 163.64 | 19.56 | 384.55 | DOW6 | -5.72 | 25.50 | 392.52 |
| DOW7 | 153.80 | 20.25 | 434.71 | DOW7 | 20.48 | 26.46 | 417.84 |
| DOW8 | 170.90 | 20.40 | 325.55 | DOW8 | 1.16 | 20.58 | 410.62 |
| Non-Clear Morning IOP1 | | | | Non-Clear Morning IOP2 | | | |
| Site Name | CTP (J/kg) | HI _{low} (K) | LCL Deficit (m) | Site Name | CTP (J/kg) | HI _{low} (K) | LCL Deficit (m) |
| ISS2 | 115.62 | 23.14 | 444.13 | ISS2 | 110.00 | 9.51 | 91.07 |
| ISS3 | 124.34 | 22.85 | 443.83 | ISS3 | 84.58 | 7.72 | 24.93 |
| DOW6 | 143.31 | 23.70 | 601.86 | DOW6 | 92.68 | 10.18 | 186.25 |
| DOW7 | 129.00 | 24.12 | 691.91 | DOW7 | 83.19 | 9.40 | 211.40 |
| DOW8 | 112.79 | 22.34 | 559.22 | DOW8 | 79.49 | 9.86 | 61.05 |
| Non-Clear Afternoon IOP1 | | | | Non-Clear Afternoon IOP2 | | | |
| Site Name | CTP (J/kg) | HI _{low} (K) | LCL Deficit (m) | Site Name | CTP (J/kg) | HI _{low} (K) | LCL Deficit (m) |
| ISS2 | 116.47 | 22.70 | 280.17 | ISS2 | 119.03 | 8.65 | -9.31 |
| ISS3 | 114.18 | 21.68 | 429.26 | ISS3 | 118.91 | 8.92 | -60.46 |
| DOW6 | 90.32 | 20.37 | 536.00 | DOW6 | 112.25 | 8.89 | -154.58 |
| DOW7 | 93.55 | 20.59 | 534.71 | DOW7 | 95.89 | 9.73 | -295.74 |
| DOW8 | 101.12 | 21.64 | 528.74 | DOW8 | 96.52 | 9.71 | -109.24 |

775

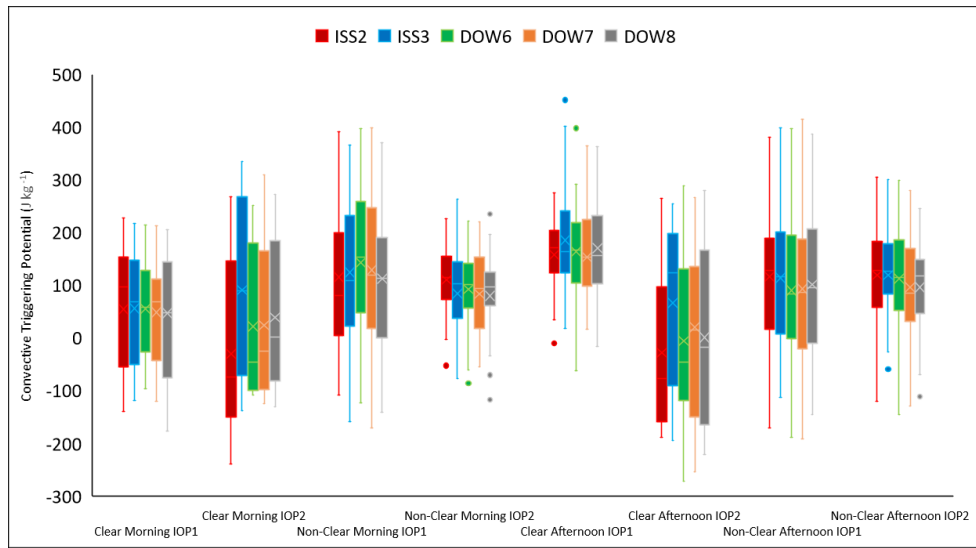
776

777

778

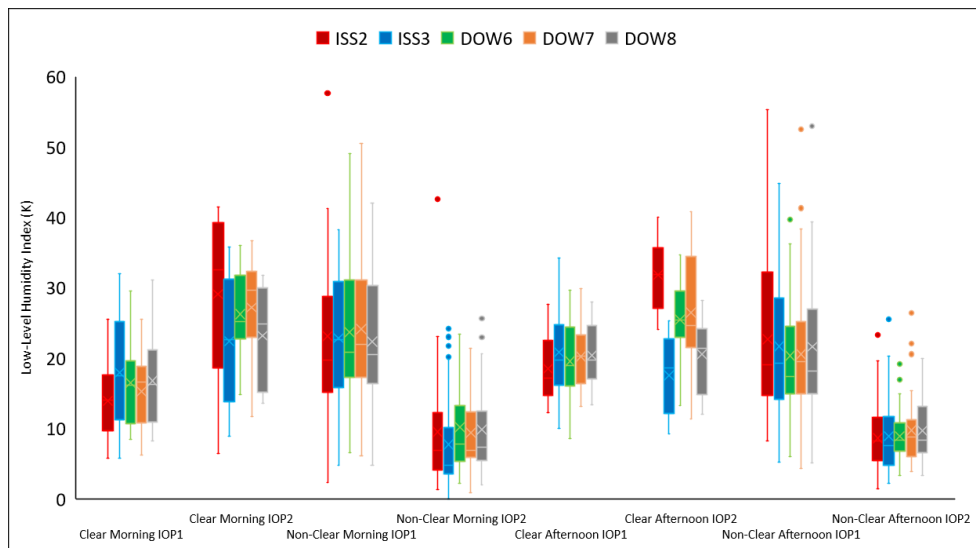
779

780 a)



781

782 b)



783

784

785

786

787

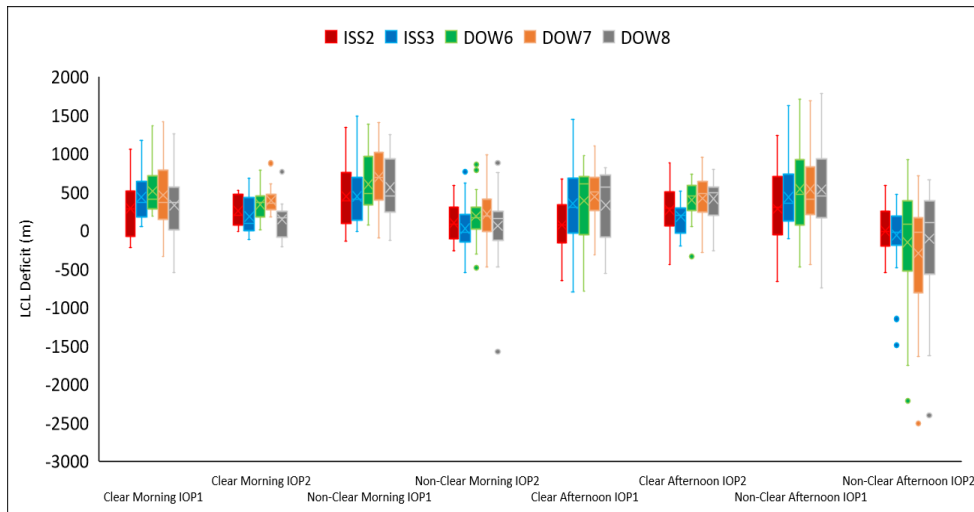
788

789

790

791

792 c)



793

794

795 Figure 7: Box and whisker plots of: a) CTP, b) HI_{low} , and c) LCL Deficit by IOP, cloud cover,
796 and time of day. Boxes with different colors represent radiosonde launching sites, which are
797 identified at the top of each panel. ISS3 and DOW8 are *irrigated* locations, ISS2 and DOW7 are
798 *non-irrigated*, and DOW6 is a *transitional* land use zone (from irrigated to non-irrigated).

799

800 A further summary of the results is presented in Figure 8 a-l with a focus on IOP2 when
801 irrigation impacts are most prominent. The CTP and HI_{low} values and observed data from the
802 three DOW sites were used and supplemented by two nearby National Weather Service operated
803 radars (the KOAX and KUEX). These data were used to determine whether convection was
804 possible and identify observed convection. Data were aggregated under three categories:

805

806

807

808

809

810

811

812

813

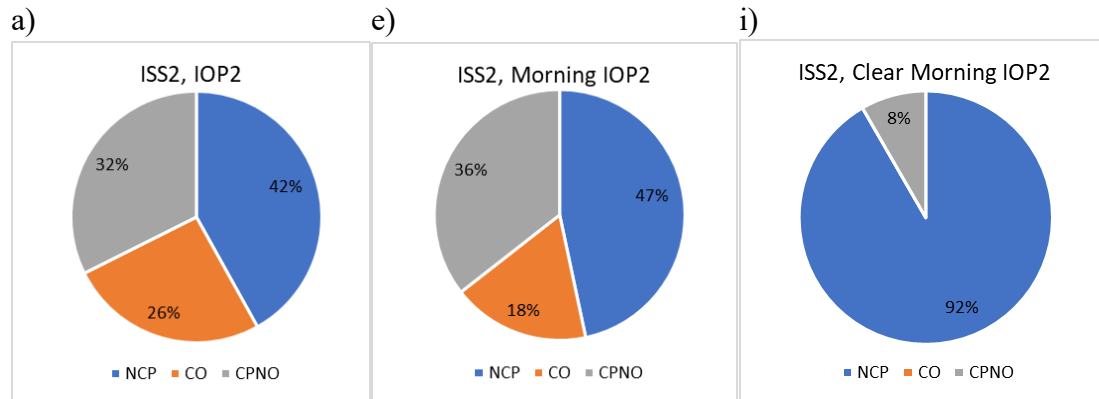
814

815

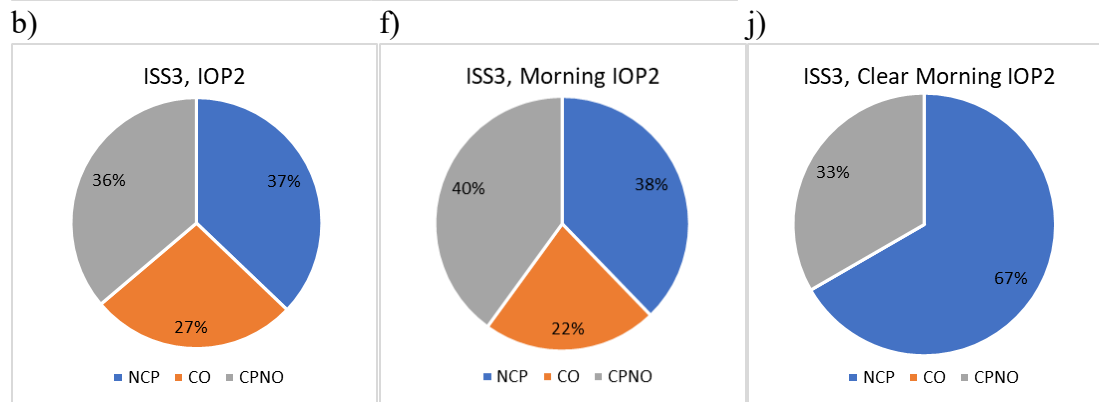
816

817

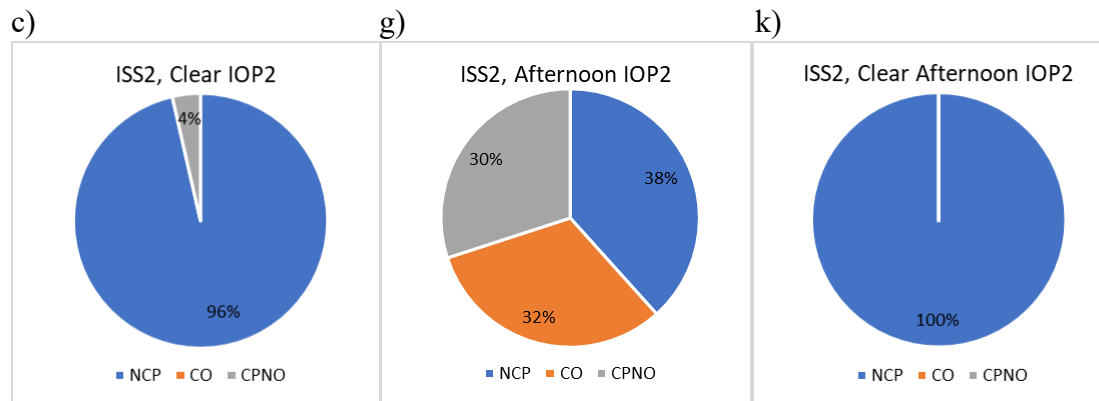
818
819



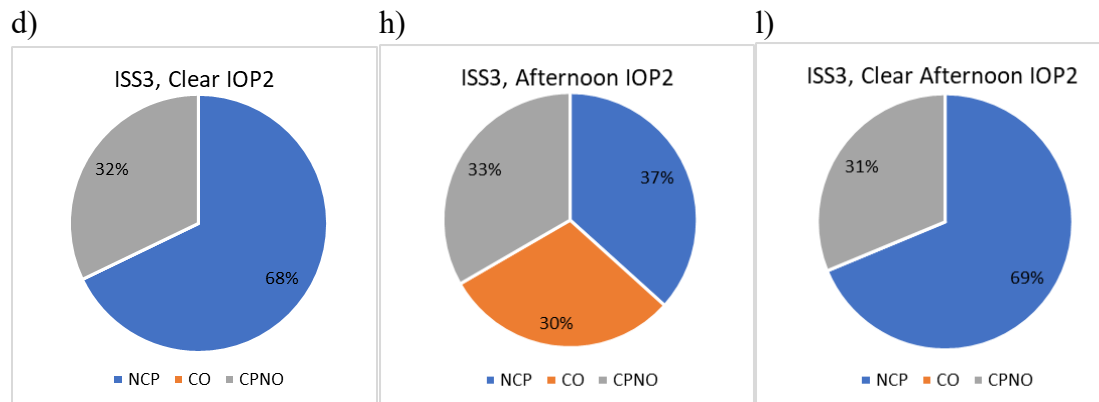
820
821



822
823



824
825



826
827

828 Figure 8: Convective possibilities for: a) ISS2, IOP2; b) ISS3, IOP2; c) ISS2, clear IOP2;
829 d) ISS3, clear IOP2; e) ISS2, morning IOP2; f) ISS3, morning IOP2 g) ISS2, afternoon IOP2; h)
830 ISS3, afternoon IOP2; i) ISS2, clear morning IOP2; j) ISS3, clear morning IOP2; k) ISS2, clear
831 afternoon IOP2; and l) ISS3, clear afternoon IOP2. NCP is no convection possible, CO is
832 convection observed, and CPNO is convection possible but not observed. ISS3 and ISS2 are
833 *irrigated* and *non-irrigated* locations, respectively.

834 no convection possible (NCP), convection observed (CO), and convection possible but not
835 observed (CPNO). When a CTP value was negative and or a HI_{low} value was 15 or higher, it was
836 concluded that conditions were not favorable for convection. In other words, an atmosphere that
837 was either too dry or too stable for precipitation to occur (Table 1). When a CTP and HI_{low} value
838 fulfilled any of the other categories, but there was no convection observed from a 2-hour span
839 between soundings, then it was identified that convection was possible, but not observed
840 (CPNO). Otherwise, there was observed convection (CO).

841 Overall (without separating the data between clear and non-clear days and between
842 morning and afternoon), it is found that, compared to non-irrigated land use, total CO was only
843 1% higher over irrigated areas during IOP2 (Figure 8 a-b). However, compared to non-irrigated
844 land use, CPNO observations were 4% higher over irrigated land use (Figure 8a-b). In addition,
845 when we separate the data by clear and non-clear days, we have found that CPNO were 28%
846 higher over irrigated areas (Figure 8 c-d).

847 On the other hand, when coupling metrics and radar observations were assessed for all
848 mornings, frequency of CO and CPNO were 4% higher while NCO was 9% lower for irrigated
849 land use (Figure 8 e-f). Thus, in this case, irrigated land use favors convection. For all afternoons
850 (not separating between clear and non-clear days) irrigated land use favors convection slightly
851 more (CO + CPNO) than non-irrigated land use (Figure 8 g-h). However, when we assess
852 observations from clear mornings, the frequency of CPNO was 25% higher over irrigated areas
853 (Figure 9i-j) while it was 31% higher during afternoons (Figure 8 k-l). Hence, irrigated land use
854 was favoring convective development during clear conditions, regardless of morning or
855 afternoon.

856

857 **4. Discussion**

858 L-A interactions are complex. Irrigated land use land cover (LULC) and the resultant
859 increase in soil moisture adds further intricacies to this relationship. The unique GRAINEX
860 dataset allowed us, for the first time, to investigate L-A interactions over irrigated and non-
861 irrigated conditions side-by-side and for different atmospheric conditions [clear vs. cloudy, with
862 latter sometimes under larger scale synoptic and advective influences], different periods of the
863 growing season, and throughout the day (e.g., morning vs. afternoon). Irrigation, and the
864 resultant increase in soil moisture, creates a wet soil advantage and favors wet coupling due to
865 modified heat flux partitioning and via L-A feedback (Roundy and Santanello 2017).

866 This paper quantified L-A interactions under a wide variety of conditions using a
867 framework developed by Findell and Eltahir (2003a, b) and the formulation modified by
868 Ferguson and Wood (2011). A key advantage of this study is that it used radiosonde data
869 collected throughout the day (8 observations per day) as opposed to only morning data (one
870 observation per day) used by Findell and Eltahir (2003a, b). Hence, data collected during
871 GRAINEX allowed us to expand on the Findell and Eltahir (2003a, b) and investigate L-A
872 interactions and irrigation's influence during the latter part of the day (e.g., afternoon) when
873 convection typically develops.

874 However, it should be noted that the CTP methodology of Findell and Eltahir (2003a, b)
875 was developed with morning soundings in mind, in which the effect of the residual
876 thermodynamic structure from the previous night is included. While the morning CTP can still
877 be interpreted using the theoretical framework developed by Findell and Eltahir (2003a), the
878 CTP from the afternoon soundings is different given that the boundary layer has already
879 developed at that point. CTP during the afternoon still represents the same physical quantity as
880 the morning CTP, however the interpretation of the value is different given that CTP is no longer
881 representative of the residual boundary layer's properties, but rather of the developed boundary
882 layer of that day. So rather than looking at CTP as representing the potential for convection later
883 in the day, it is representative of how the boundary layer developed through the day (towards a
884 dry adiabatic profile in the case of larger CTP values compared to morning or maintaining a
885 moist adiabatic profile in the case of smaller afternoon CTP values). Thus, the afternoon CTP
886 aids in identification of when sensible (in the case of larger afternoon CTP values) or latent (in

887 the case of smaller afternoon CTP values) heat fluxes are driving boundary layer property
888 changes throughout the day.

889 It is well known that favorable conditions for convective development (and precipitation)
890 can occur due to: 1) advection of moisture linked to large-scale circulation, 2) utilization of
891 moisture linked to local sources including land use (irrigation in this case), and 3) a combination
892 of both. It is also possible that the large-scale influence dominates and overshadows/suppresses
893 local (e.g., land use/irrigation) influences on low-level atmospheric development and any
894 resultant precipitation. In this study, it was found that irrigation's influence can be sufficiently
895 large so that it provides favorable environment for convection and cloud development under a
896 variety of conditions.

897 Results suggest that, with a few exceptions, the transition from the early growing season
898 (early June/early summer) to the peak growing season (late July/peak summer) leads to a decline
899 in CTP, HI_{low} , and LCL Deficits. In other words, as we moved from IOP1 to IOP2, average CTP,
900 HI_{low} , and LCL Deficits all decreased. Although CTP declined, it was well above zero in all
901 cases. As a result, the CTP values during IOP2, along with lower HI_{low} and LCL Deficit offered
902 overall favorable conditions for convection. Additionally, with the transition from the early
903 summer (IOP1) to the peak summer (IOP2) and increased irrigation, conditions became more
904 favorable for convective development over irrigated land use. Note that ISS2 and ISS3 are
905 located over non-irrigated and irrigated land use, respectively. The DOW sites are located in the
906 irrigated (DOW8), non-irrigated (DOW7), and in the boundary between irrigated and non-
907 irrigated land uses (transitional) (DOW6). LCL Deficits during IOP1 were the lowest for non-
908 irrigated land use and the highest for the transition zone between irrigated and non-irrigated land
909 use. During IOP1, naturally occurring soil moisture was higher over non-irrigated land use (e.g.,
910 Figure 3c, Rappin et al. 2021), which supports the rainfed agriculture. This also leads to higher
911 ET and result in a lower LCL Deficit. On the other hand, for IOP2, HI_{low} values for irrigated
912 ISS3 were the lowest of all the sites. This suggests that the increase in moisture due to irrigation
913 resulted in lower HI_{low} for the ISS3 site compared to all other sites. Thus, land use impacted the
914 convective environment with the effect further evident during IOP2 when irrigation is
915 widespread (e.g., Figure 3c, Rappin et al. 2021).

916 After aggregating the metrics by IOPs, LCL Deficit and HI_{low} show a statistically
917 significant difference between irrigated and non-irrigated land use for clear days during IOP1

918 and IOP2. Similar results were found for CTP but only during IOP2. Clear days in IOP1
919 observed higher HI_{low} over irrigated land use compared to the other sites. Additionally, over
920 irrigated land use, LCL Deficits were higher than non-irrigated land use. This changed with clear
921 days in IOP2 where HI_{low} and LCL Deficits were lower over irrigated land use compared to non-
922 irrigated. For non-clear days in IOP1 and IOP2, differences in CTP and HI_{low} were not
923 statistically significant between irrigated and non-irrigated land use. However, LCL Deficits
924 showed statistically significant differences during non-clear days in IOP1, with irrigated land use
925 reporting lower LCL Deficits than non-irrigated cropland. These results were impacted by the
926 presence of synoptic forcing causing similarities in the results.

927 Analyzing the metrics by day with and without cloud cover (i.e., clear vs. non-clear)
928 allows for an understanding of cloud cover impacts on CTP, HI_{low} , and LCL Deficits in the
929 context of land use (irrigated vs. non-irrigated). Note that cloud cover can indicate the presence
930 of large-scale synoptic influence. It is found that during cloudy days (regardless of time of the
931 growing season, i.e., IOP1 or IOP2) differences in CTP, HI_{low} , and LCL Deficits over irrigated
932 versus non-irrigated land use are statistically not significant. On the other hand, for clear days,
933 differences in CTP, HI_{low} , and LCL Deficits over irrigated and non-irrigated land use are
934 statistically significant. The CTP and HI_{low} values for the transitional land use area were
935 generally in between, compared to values from irrigated and non-irrigated areas.

936 Aggregating and analyzing the metrics by time of day shows increases in CTP for the ISS
937 sites from morning to afternoon. These changes were not observed in the DOW sites. Changes in
938 HI_{low} from morning to afternoon were negligible for all sites. As expected, LCL Deficits
939 decreased from morning to afternoon with the diurnal cycle enhancing mixing and thus PBLH
940 increased and the LCL Deficit decreased.

941 Analyzing the data by time of day and IOP, it was found that the difference in morning
942 CTP values between irrigated and non-irrigated land use were not statistically significant for
943 IOP1 and IOP2. However, differences in LCL Deficit between irrigated and non-irrigated land
944 use for IOP1 and IOP2 mornings were statistically significant. LCL Deficits during mornings in
945 IOP1 (IOP2) were the lowest for non-irrigated (irrigated) land use. The LCL Deficit values for
946 the afternoons were notably lower for all sites during IOP2 when irrigation was widespread.

947 However, non-irrigated ISS2 and irrigated ISS3 observed the highest and one of the lowest LCL
948 Deficit values, respectively. Compared to IOP1 and overall, HI_{low} values were favorably lower
949 during IOP2. The irrigated ISS3 and DOW8 sites observed two of the lowest values of HI_{low} in
950 the morning and afternoon, indicating more favorable conditions for convection over irrigated
951 land use.

952 The role of cloud cover and time of day were also considered in the context of L-A
953 interactions. Differences in CTP between irrigated and non-irrigated sites were statistically
954 significant for both clear mornings and clear afternoons, where CTP values were higher for
955 irrigated land use compared to non-irrigated. For clear afternoons, HI_{low} was favorably lower
956 over irrigated land use compared to non-irrigated. For non-clear mornings and afternoons,
957 observed differences for CTP and HI_{low} over irrigated and non-irrigated land use were
958 statistically not significant. However, the LCL Deficits during non-clear mornings were
959 statistically significantly different, with irrigated land use observing a lower LCL Deficit
960 compared to non-irrigated. Again, it is evident that under clear conditions irrigated land use
961 provides a more favorable environment for convective development. After further analyzing the
962 coupling metrics by IOPs, cloud cover, and time of day, results show similar impacts. Based on
963 the CTP and LCL Deficit, it can be noted that even under non-clear conditions (i.e., under large-
964 scale synoptic influence) the influence of irrigation for convective development is noticeable.

965 Overall, there is one sustained factor that influenced these three L-A coupling metrics and
966 thus the convective environment: irrigation and the related increase in surface moisture.
967 Increases in surface moisture leads to increases in CTP and favorable decreases in HI_{low} and LCL
968 Deficit over irrigated land use. The impacts of irrigation are most prominent during IOP2 (in
969 other words the peak growing period) when application of irrigation increases, leading to
970 increased soil moisture. It is clear that land use and vegetation cover/crop growth phases
971 (represented by IOP1 and IOP2) are a dominant influence on L-A interactions and altered
972 convective potential.

973

974

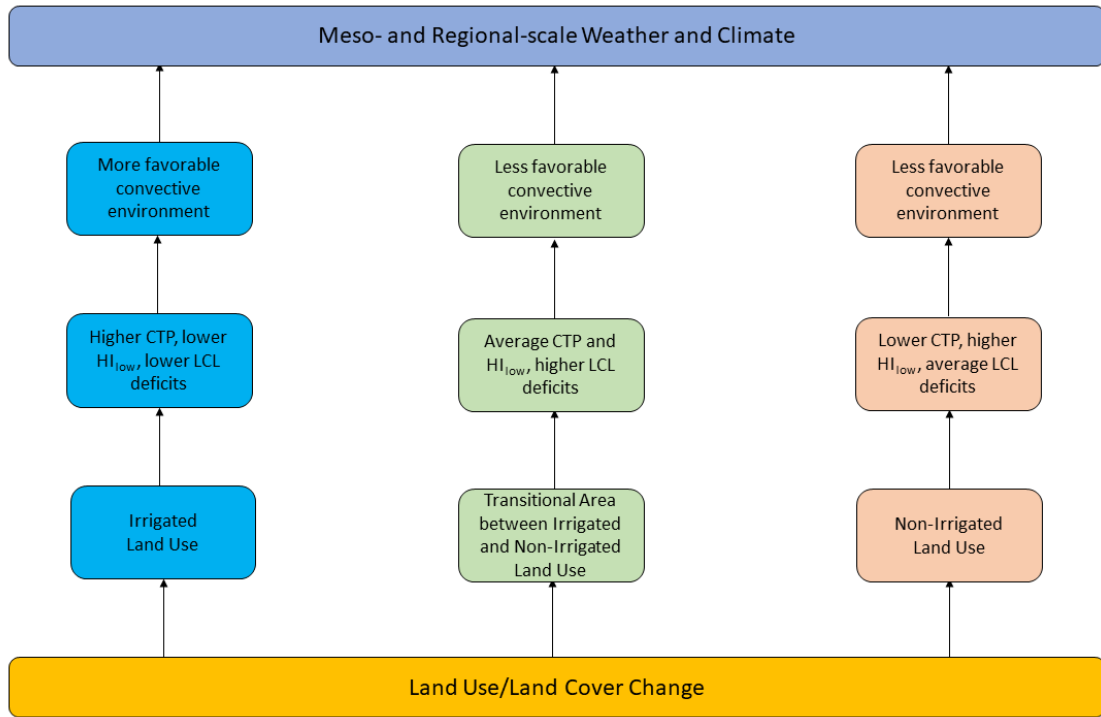
975

976 **5. Summary Remarks**

977 LULCC and substantial irrigation expansion took place during the second half of 20th
978 century in Nebraska and elsewhere. To better understand the impacts of irrigation on L-A
979 interactions the GRAINEX field campaign was conducted. The data from the field campaign was
980 used to calculate three L-A coupling/interaction metrics, including CTP, HI_{low} , and LCL Deficit
981 to quantify the influence of irrigated and non-irrigated land use on the lower atmosphere and
982 convection.

983 Composites of CTP, HI_{low} , and LCL Deficits were calculated for two 15-day periods of
984 the growing season of 2018. Over 1000 soundings launched over these two periods (total of 30-
985 day) were used to calculate CTP, HI_{low} , and LCL Deficit. As shown in table 2, these calculations
986 (i.e., metrics') were then grouped by IOP (IOP1 and IOP2), cloud cover (clear and non-clear
987 days), cloud cover (clear and non-clear days (during IOP1 and IOP2, time of day, time of day
988 and IOP1 and IOP2, and time of day, cloud cover (clear and non-clear day) and IOP1 and IOP2.
989 The analyses were completed to further understand the land surface influence on the convective
990 environment. We recognize that in some cases 'clean' separation of clear versus non-clear days
991 may not be as clean. Nonetheless, we are confident that our results are satisfactory because they
992 agree with the conceptual understanding of L-A interactions under irrigated and non-irrigated
993 land uses.

994
995 This study finds that with higher CTP, lower HI_{low} , and lower LCL Deficit, irrigated land
996 use will yield a more favorable environment for convection. When separated by IOPs, HI_{low} was
997 found to be lower for irrigated cropland compared to non-irrigated land use (Table 3). When
998 separated by cloud cover, CTP values were found to be higher over irrigated cropland compared
999 to non-irrigated land use. Compared to non-irrigated land use, LCL Deficits during the peak
1000 growing season (IOP2) are favorably lower over irrigated land use, which is conducive for
1001 convection (Table 4, Table 5, and Table 6). Figure 9 summarizes the findings of this research.



1002

1003 Figure 9: Summary of the impacts of LULCC on L-A coupling metrics and convective
 1004 outcomes.

1005

1006 Irrigation’s relationship with weather and climate is complex, but the observations from
 1007 GRAINEX and analyses completed for this research have made this relationship clearer.
 1008 However, further analysis of GRAINEX data and supporting meso-scale modeling research
 1009 needs to be undertaken to gather new insight on meso-scale circulations in the context of
 1010 LULCC and irrigation. In addition, a ‘climatology’ is established for one growing season.
 1011 Analysis of data for additional growing seasons would be helpful to better understand the
 1012 connections between irrigation, land use, and convection.

1013 In this vein, nocturnal convection is common for southcentral and southeast Nebraska
 1014 (Reif and Bluestein 2017; Geert et al. 2017). It is shown in this and other GRAINEX data-based
 1015 studies (Rappin et al. 2021; Lachenmeier et al. 2024) that irrigation can result in higher near
 1016 surface and lower tropospheric moisture content. We suggest that the elevated moisture content
 1017 due to irrigation may potentially interact with nocturnal processes and impacts nocturnal
 1018 convection. The radiosonde observations during GRAINEX were primarily focused on daytime.
 1019 In the future, new research using nighttime observations would assist in further understanding of

1020 the role of irrigation on nocturnal convection. Future research may also include modeling studies
1021 to understand the impacts of irrigation on selected and representative weather conditions.
1022 Moreover, seasonal-scale modeling research needs to be undertaken to better understand
1023 downstream impacts of irrigation on precipitation.

1024

1025

1026

1027

1028 **Acknowledgments.** The authors would like to thank three anonymous reviewers for their
1029 valuable feedback which helped to improve this manuscript. This research is funded by the
1030 National Science Foundation (NSF) Grants AGS-1853390 (Rezaul Mahmood and Eric Rappin),
1031 AGS-1720477 (Udaysankar Nair), and AGS-1552487 (Roger Pielke Sr.). Mention of trade
1032 names or commercial products in this publication is solely for the purpose of providing specific
1033 information and does not imply recommendation or endorsement by the U.S. Department of
1034 Agriculture. USDA is an equal opportunity provider and employer.

1035

1036 **Data Availability Statement:** Data used in this study can be found in:

1037 https://www.eol.ucar.edu/field_projects/grainex.

1038

1039

1040

1041

1042

1043

1044

1045 **References**

- 1046 Adegoke, J.O., R. A. Pielke, J. Eastman, R. Mahmood, and K. G. Hubbard, 2003: Impact of
1047 irrigation of midsummer surface fluxes and temperature under dry synoptic conditions: A
1048 regional atmospheric model study of the U.S. High Plains. *Mon. Wea. Rev.* **131**,
1049 556-564.
- 1050
1051 Alter, R. E., H. C. Douglas, J. M. Winter, and E. A. Eltahir, 2018: Twentieth century regional
1052 climate change during the summer in the Central United States attributed to agricultural
1053 intensification. *Geophys. Res. Lett.*, **45**, 1586-1594.
- 1054
1055 Alter, R. E., E.-S., Im, and E. A. B. Eltahir, 2015: Rainfall consistently enhanced around the
1056 Gezira scheme in East Africa due to irrigation. *Nature Geosci.*, **8**, 763–767.
- 1057
1058 Barnston, A., and P. T. Schickedanz, 1984: The effect of irrigation on warm season precipitation
1059 in the Southern Great Plains. *J. Climate Appl. Meteorol.*, **23**, 865–888.
- 1060
1061 Berg, A., K. Findell, B. R. Lintner, P. Gentine, and C. Kerr, 2013: Precipitation sensitivity to
1062 surface heat fluxes over North America in reanalysis and model data. *J. Hydrometeorol.* **14**,
1063 722-743.
- 1064
1065 Betts, A. K., and J. H. Ball, 1998: FIFE surface climate and site-average dataset 1987-89.
1066 *J. Atm. Sci.* **55**, 1091-1108.
- 1067
1068 Bonfils, C., and D. Lobell, 2007: Empirical evidence for a recent slowdown in irrigation-induced
1069 cooling. *Proc. Natl. Acad. Sci. USA*, **104**, 13582–13 587,
- 1070
1071 Chen, L., and P. A. Dirmeyer, 2019: Global observed and modelled impacts of irrigation on
1072 surface temperature. *Int. J. Climatol.* **39**, 2587–2600. <https://doi.org/10.1002/joc.5973>
- 1073
1074 Christy, J. R., W. B. Norris, K. Redmond, and K. P. Gallo, 2006: Methodology and results of
1075 calculating central California surface temperature trends: Evidence of human-induced
1076 climate change? *J. Climate*, **19**, 548–563,
- 1077
1078 Collow, T.W., A. Robock, and W. Wu, 2014: Influences of soil moisture and vegetation on
1079 convective precipitation forecasts over the United States Great Plains. *J. Geophys. Res.*
1080 *Atmos.*, **119**, 9338–9358, doi:10.1002/2014JD021454.
- 1081
1082 Cook, B. I., M. J. Puma, N. Y. Krakauer, 2011: Irrigation induced surface cooling in the context
of modern and increased greenhouse gas forcing. *Clim. Dyn.* **37**, 1587–1600.
- 1083
1084 Cook, B. I., S. P. Shukla, M. J. Puma, and L. S. Nazarenko, 2015: Irrigation as an historical
1085 climate forcing. *Clim. Dyn.*, **44**, 1715–1730. <https://doi.org/10.1007/s00382-014-2204-7>
- 1086
1086 Cook, B. I., S. S. McDermid, M. J. Puma, A. P. Williams, R. Seager, M. Kelley, L. Nazarenko,

1087 and I. Aleinov 2020: Divergent regional climate consequences of maintaining current
1088 irrigation rates in the 21st century. *J. Geophys. Res.*, **125**, e2019JD031814.
1089 <https://doi.org/10.1029/2019JD031814>
1090

1091 DeAngelis, A., F. Dominguez, Y. Fan, A. Robock, M. D. Kustu, and D. Robinson, 2010:
1092 Evidence of enhanced precipitation due to irrigation over the Great Plains of the United
1093 States. *J. Geophys. Res.*, **115** (D15115). doi:10.1029/2010JD013892
1094

1095 Earth Observing Laboratory, 2020: GRAINEX: The Great Plains Irrigation Experiment.
1096 Accessed 11 June 2022. https://www.eol.ucar.edu/field_projects/grainex
1097

1098 Ek, M., and A. A. M. Holtslag, 2004: Influence of soil moisture on boundary layer cloud
1099 development. *J. Hydrometeor.*, **5**, 86–99.
1100

1101 Eltahir, E. A. 1998: A soil moisture–rainfall feedback mechanism: 1. Theory and observations.
1102 *Water Res. Res.* **34**, 765-776.
1103

1104 Fan, X., Z. Ma, Q. Yang, Y. Han, and R. Mahmood, and Z. Zheng, 2015a: Land use/land
1105 cover changes and regional climate over the Loess Plateau during 2001-2009 – Part I.
1106 Observed evidences. *Clim. Change* **129**, 427-440. DOI 10.1007/s10584-014-1069-4.
1107

1108 Fan, X., Z. Ma, Q. Yang, Y. Han, and R. Mahmood, 2015b: Land use/land cover
1109 changes and regional climate over the Loess Plateau during 2001-2009 – Part II.
1110 Interrelationship from observations. *Clim. Change* **129**, 441-455. DOI 10.1007/s10584-
1111 014-1068-5.
1112

1113 Flanagan, P., R. Mahmood, T. Sohl, M. Svoboda, B. Wardlow, M. Hayes, and E. Rappin, 2021:
1114 Atmospheric response to four projected land use land cover change scenarios for
1115 2050 in the North Central United States. *Earth Inter.* **25**, 177-194.
1116

1117 Ferguson, C.R., and Wood, E.F., 2011: Observed land-atmospheric coupling from
1118 satellite remote sensing and reanalysis. *J. Hydrometeor.*, **12**, 1221-1254.

1119 Findell, K.L., and Eltahir, E.A.B., 2003a: Atmospheric controls on soil moisture-
1120 boundary layer interactions. Part I: Framework development. *J. Hydrometeor.*,
1121 **4**, 552-569.

1122 Findell, K.L., and Eltahir, E.A.B., 2003b: Atmospheric controls on soil moisture-
1123 boundary layer interactions. Part II: Feedbacks within the continental United
1124 States. *J. Hydrometeor.*, **4**, 570-583.
1125

1126 Findell, K. L., and E. A. Eltahir, 2003c: Atmospheric controls on soil moisture-boundary layer
1127 interactions: Three-dimensional wind effects. *J. Geophys. Res.* **108**,
1128 DOI: 10.1029/2001JD001515.
1129

1130 Ford, T. W., A. D. Rapp, and S. M. Quiring, 2015a: Does afternoon precipitation occur
1131 preferentially over dry or wet soils in Oklahoma? *J. Hydrometeor.* **16**,

1132 874–888.
1133
1134 Ford, T. W., A. D. Rapp, S. M. Quiring, and J. Blake, 2015b: Soil moisture–precipitation
1135 coupling: Observations from the Oklahoma Mesonet and underlying physical
1136 mechanisms. *Hydrol. Earth Sys. Sci.* **19**, 3617–3631.
1137
1138 Frye, J.D. and T. Mote, 2010: Convection initiation along soil moisture boundaries in the
1139 Southern Great Plains. *Mon. Wea. Rev.*, **138**, 1140–1151.
1140
1141 Geert, B., D. Parsons, C. L. Ziegler, T. M. Weckwerth, M. I. Biggerstaff, R. D. Clark,
1142 M. C. Coniglio, B. B. Demoz, R. A. Ferrare, W. A. Gallus Jr., K. Haghi, J. M. Hanesiak,
1143 P. M. Klein, K. R. Knupp, K. Kosiba, G. M. McFarquhar, J. A. Moore, A. R. Nehrir,
1144 M. D. Parker, J. O. Pinto, R. M. Rauber, R. S. Schumacher, D. D. Turner, Q. Wang,
1145 X. Wang, Z. Wang, and J. Wurman 2017: The 2015 Plains Elevated Convection At Night
1146 (PECAN) field project. *Bull. Amer. Meteor. Soc.*, **98**, 767–786.
1147
1148 Harding, K. J. and P. K. Snyder, 2012a: Modeling the atmospheric response to irrigation in the
1149 Great Plains. Part I: General impacts on precipitation and the energy budget. *J.*
1150 *Hydrometeor.* **13**, 1667–1686.
1151
1152 Harding, K. J. and P. K. Snyder, 2012b: Modeling the atmospheric response to irrigation in the
1153 Great Plains. Part II: The precipitation of irrigated water and changes in precipitation
1154 recycling. *J. Hydrometeor.* **13**, 1687–1703.
1155
1156 Holt, T. R., D. Niyogi, F. Chen, K. Manning, M. A. LeMone, and A. Qureshi, 2006: Effect of
1157 land–atmosphere interactions on the IHOP 24–25 May 2002 convection case. *Mon. Wea.*
1158 *Rev.* **134**, 113–133.
1159
1160 Hu, Z., Z. Xu, Z. Ma, R. Mahmood, and Z. Yang, 2019: Potential surface hydroclimate
1161 responses to increases in greenhouse gas concentrations and land use and land cover
1162 changes. *Int. J. Climatol.* **39**, 814–827.
1163
1164 Kang, S., and E. A. B. Eltahir, 2019: Impact of irrigation on regional climate over Eastern China.
1165 *Geophys. Res. Lett.*, **46**, 5499–5505.
1166
1167 Lachenmeier, E., R. Mahmood, C. Phillips, U. Nair, E. Rappin, R. A. Pielke Sr., W. Brown,
1168 S. Oncley, J. Wurman, K. Kosiba, A. Kaulfus, J. Santanello Jr., E. Kim,
1169 P. Lawston-Parker, M. Hayes, and T. E. Franz, T. E. 2024: Irrigated agriculture
1170 Significantly modifies seasonal boundary layer atmosphere and lower tropospheric
1171 convective environment. *J. Appl. Meteor. Clim.* **63**, 245–261.
1172
1173 Lawston, P. M., J. A. Santanello Jr., B. Hanson, and K. Arsensault, 2020: Impacts of irrigation
1174 on summertime temperatures in the Pacific Northwest. *Earth Interac.*, **24**, 1–26.
1175
1176 Lawston, P. M., J. A. Santanello Jr., B. F. Zaitchik, and M. Rodell, 2015: Impact of irrigation
1177 methods on land surface model spinup and initialization of WRF Forecasts.
J. Hydrometeor. **16**, 1135–1154.
1178
1179 Lawston-Parker, P., J. A. Santanello Jr., and N. W. Chaney, 2023: Investigating the response of

1178 land-atmosphere interactions and feedbacks to spatial representation of irrigation in a
1179 coupled modeling framework. *Hydrol. Earth Syst. Sci.*, **27**, 2787–2805.

1180

1181 Leeper, R., R. Mahmood, and A. I. Quintanar, 2011: Influence of karst landscape on
1182 planetary boundary layer atmosphere: A Weather Research and Forecast (WRF) model-
1183 based investigation. *J. Hydrometeor.*, **12**: 1512-1529.

1184

1185 Lobell, D.B., and C. Bonfils, 2008: The effect of irrigation on regional temperatures: a spatial
1186 and temporal analysis of trends in California. *J. Clim.*, **21**, 2064-2071.

1187

1188 Mahmood, R., and K. G. Hubbard, 2002: Anthropogenic land-use change in the North
1189 American tall grass-short grass transition and modification of near-surface hydrologic
1190 cycle. *Clim. Res.*, **21**, 83-90.

1191

1192 Mahmood R., S. A. Foster, T. Keeling, K. G. Hubbard, C. Carlson, and R. Leeper, 2006: Impacts of
1193 irrigation on 20th century temperature in the Northern Great Plains. *Glob. Planet.*
1194 *Change*, **54**, 1-18.

1195

1196 Mahmood, R., K. G. Hubbard, and C. Carlson, 2004: Modification of growing season
1197 surface temperature records in the Northern Great Plains due to land use transformation:
1198 verification of modeling results and implication for global climate change.
1199 *Int. J. Climatol.*, **24**, 311-327.

1200

1201 Mahmood, R., T. Keeling, S. A. Foster, and K. G. Hubbard, 2013: Did irrigation impact
1202 20th century temperature in the High Plains aquifer region? *Appl. Geogr.* **38**, 11-21.

1203

1204 Mahmood, R., R. Leeper, and A. I. Quintanar, 2011: Sensitivity of planetary boundary
1205 layer atmosphere to historical and future changes of land use/land cover, vegetation
1206 fraction, and soil moisture in Western Kentucky, USA. *Glob. Planet. Change*,
1207 **78**: 36-53.

1208

1209 Mahmood, R, A. Littell, K. G. Hubbard, and J. You, 2012: Observed data-based
1210 assessment of relationships among soil moisture at various depths, precipitation, and
1211 temperature. *Appl. Geogr.*, **34**: 255-264.

1212 Mahmood, R., R. A. Pielke Sr., K. G. Hubbard, D. Niyogi, G. Bonan, P. Lawrence, B. Baker,
1213 R. McNider, C. McAlpine, A. Etter, S. Gameda, B. Qian, A. Carleton,
1214 A. Beltran-Przekurat, T. Chase, A. I. Quintanar, J. O. Adegoke, S. Vezhapparambu,
1215 G. Conner, S. Asefi, E. Sertel, D. R. Legates, Y. Wu, R. Hale, O. N. Frauenfeld, A. Watts,
1216 M. Shepherd, C. Mitra, V. G. Anantharaj, S. Fall, R. Lund, A. Nordfelt, P. Blanken, J. Du,
1217 H-I., Chang, R. Leeper, U. S. Nair, S. Dobler, R. Deo, and J. Syktus, 2010: Impacts of land
1218 use land cover change on climate and future research priorities. *Bull. Amer. Meteor. Soc.*,
1219 **91**, 37-46.

1220

1221 Mahmood, R., Pielke, R.A., Hubbard, K.G., Niyogi, D., Dirmeyer, P.A., McAlpine, C., Carleton,
1222 A.M., Hale, R., Gameda, S., Beltrán-Przekurat, A., Baker,B., McNider, R., Legates, D.R.,
1223 Shepherd, M., Du, J., Blanken, P.D., Frauenfeld, O.W., Nair, U.S., Fall, S. 2014. Land

1224 cover changes and their biogeophysical effects on climate. *Inter. J. Climatol.* **34**, 929-953.

1225 McDermid, S. S., R. Mahmood, M. Hayes, J. E. Bell, and Z. Lieberman, 2021:
1226 Environmental trade-offs for sustainable irrigation. *Nat. Geosci.*, **14**, 706-709.

1227

1228 McDermid, S. M. Nocco, P. Lawston-Parker, J. Keune, Y. Pokhrel, M. Jain, J. Jägermeyr,
1229 L. Brocca, C. Massari, A. Jones, A., P. Vahmani, W. Thiery, Y. Yao, A. Bell, L. Chen,
1230 W. Dorigo, N. Hanasaki, J. Jasechko, Lo Min-Hui, R. Mahmood, V. Mishra,
1231 N. D. Mueller, D. Niyogi, S. Rabin, S. Sam, L. Sloat, Y. Wada, L. Zappa, F. Chen, B. I.
1232 Cook, H. Kim, D. Lombardozzi, J. Polcher, D. Ryu, J. Santanello, Y. Satoh,
1233 S. Seneviratne, D. Singh, and T. Yokohata, 2023: Irrigation in the Earth system. *Nat.*
1234 *Rev. Earth Environ.*, <https://doi.org/10.1038/s43017-023-00438-5>

1235

1236 McPherson, R. A. 2007: A review of vegetation—atmosphere interactions and their influences
1237 on mesoscale phenomena. *Prog. Phys. Geogr.* **31**, 261-285.

1238

1239 Mueller, N. D., E. E. Butler, K. A. McKinnon, A. Rhines, M. P. Tingley, N. M. Holbrook, and
1240 P. Huybers, 2016: Cooling of US Midwest summer temperature extremes from cropland
1241 intensification. *Nat. Climate Change*, **6**, 317–322, doi:10.1038/nclimate2825.

1242

1243 Mueller, N.D., A. Rhines, E. E. Butler, D. K. Ray, S. Siebert, N. M. Holbrook, and P. Huybers,
1244 2017: Global relationships between cropland intensification and summer temperature
1245 extremes over the last 50 years. *J. Clim.*, **30**, 7505-7528.

1246

1247 Nair, U. S., E. Rappin, E. Foshee, W. Smith, R. A. Pielke Sr., R. Mahmood, R., J. L. Case,
1248 C. B. Blankenship, M. Shepherd, J. A. Santanello, and D. Niyogi, 2019: Influence
1249 of land cover and soil moisture based brown ocean effect on an extreme rainfall event
1250 from a Louisiana Gulf Coast tropical System. *Sci Rep.*, **9**, 17136.

1251

1252 National Centers for Environmental Information, 2022. Radar. Accessed 29 September 2022.
1253 <https://www.ncei.noaa.gov/products/radar>

1254 Nikiel, C.A., and E. A. B. Eltahir, E.A.B. 2019. Summer climate change in the Midwest and
1255 Great Plains due to agriculture during the twentieth century. *J. Clim.*, **32**, 5583-5599.

1256

1257 Ookouchi, Y., M. Segal, R.C. Kessler, and R.A. Pielke, 1984: Evaluation of soil moisture effects
1258 on the generation and modification of mesoscale circulations. *Mon. Wea. Rev.*, **112**,
1259 2281-2292.

1260

1261 Pei, L., N. Moore, S. Zhong, A. D. Kendall, Z. Gao, and D. W. Hyndman, 2016: Effects of
1262 Irrigation on summer precipitation over the United States. *J. Clim.*, **29**, 3541-3558.

1263

1264 Phillips, C.E., U. S. Nair, R. Mahmood, E. Rappin, and R. A. Pielke Sr., 2022: Influence of
1265 irrigation on diurnal mesoscale circulations: results from GRAINEX. *Geophys.*
Res. Lett., **49**, e2021GL096822

1266

1267 Pielke Sr., R.A., A. Pitman, D. Niyogi, R. Mahmood, C. McAlpine, F. Hossain,
K. Klein Goldewijk, U. Nair, R. Betts, S. Fall, M. Reichstein, P. Kabat, and

1268 N. de Noblet-Ducoudré, 2011: Land use/land cover changes and climate: Modeling
1269 analysis and observational evidence. *Wiley Interdisc. Rev.: Clim. Change* **2**, 828-850.
1270

1271 Pielke, R.A., Mahmood, R., McAlpine, C. 2016. Land’s complex role in climate change.
1272 *Phys. Today*, 69, 40-46.

1273 Pielke, R.A., and X. Zeng, 1989: Influence on severe storm development of irrigated land.
1274 *Nat. Wea. Digest*, **14**, 16-17.

1275 Puma, M. J., and B. J. Cook, 2010: Effects of irrigation on global climate during the 20th
1276 century. *J. Geophys. Res.*, **115**, D16120. DOI: 10.1029/2010JD014122.
1277

1278 Rappin, E., R. Mahmood, U. Nair, R. A. Pielke Sr, W. Brown, S. Oncley, J. Wurman,
1279 K. Kosiba, Kaulfus, C. Phillips, E. Lachenmeier, J. Santanello, E. Kim, and
1280 P. Lawston-Parker, 2021: The Great Plains Irrigation Experiment (GRAINEX). *Bull.*
1281 *Amer. Meteor. Soc.*, 102: ES1756-1785.
1282

1283 Rappin, E. D., R. Mahmood, U. S. Nair, and R. A. Pielke Sr., 2022: Land-atmosphere
1284 interactions during GRAINEX: planetary boundary layer evolution in the presence of
1285 irrigation. *J. Hydrometeor.*, **23**, 1401-1417.
1286

1287 Reif, D. W., and H. B. Bluestein, 2017: A 20-Year Climatology of Nocturnal Convection
1288 Initiation over the Central and Southern Great Plains during the Warm Season. *Mon.*
1289 *Wea. Rev.*, **145**, 1615–1639
1290

1291 Rodgers, W., R. Mahmood, R. Leeper, and J. Yan, J. 2018: Land cover change, surface
1292 mining, and their impacts on a heavy rain event in the Appalachia. *Annals*
1293 *Amer. Assoc. Geogr.* **108**, 1187-1209.
1294
1295

1296 Santanello Jr., J. A., P. A. Dirmeyer, C. R. Ferguson, K. L. Findell, A. B. Tawfik, A. Berg,
1297 M. Ek, P. Gentine, B. P. Guillod, C. van Heerwaarden, J. Roundy, and V. Wulfmeyer,
1298 2018: Land–atmosphere interactions: The LoCo perspective. *Bull. Amer. Meteor. Soc.*,
1299 **99**, 1253–1272.
1300

1301 Santanello Jr., J. A., M. A. Friedl, and M. B. Ek, 2007: Convective planetary boundary layer
1302 interactions with the land surface at diurnal time scales: Diagnostics and feedbacks.
1303 *J. Hydrometeor.* **8**, 1082-1097.
1304

1305 Santanello Jr., J. A., P. Lawston, S. V. Kumar, E. Dennis, 2019: Understanding the impacts
1306 of soil moisture initial conditions on NWP in the context of land–atmosphere
1307 coupling. *J. Hydrometeor.* **20**, 793-819.
1308

1309 Santanello Jr., J. A., C. D. Peters-Lidard, S. V. Kumar, C. Alonge, and W. K. Tao, 2009: A
1310 modeling and observational framework for diagnosing local land–atmosphere coupling
1311 on diurnal time scales. *J. Hydrometeor.* **10**, 577-599.
1312

1313 Santanello Jr., J. A., C. D. Peters-Lidard, and S. V. Kumar, 2011: Diagnosing the sensitivity of
1314 local land-atmosphere coupling via the soil moisture-boundary layer interaction.
1315 *J. Hydrometeor.*, **12**, 766-786.
1316

1317 Santanello Jr., J. A., C. Peters-Lidard, A. D. Kennedy, and S. V. Kumar, 2013: Diagnosing the
1318 nature of land-atmosphere coupling during the 2006-7 dry/wet extremes in the US
1319 southern Great Plains. *J. Hydrometeor.* **14**, 3-24.
1320

1321 Schlemmer, L., C. Hohenegger, J. Schmidli, C. S. Bretherton, and C. Schär, 2011: An
1322 Idealized cloud-resolving framework for the study of midlatitude diurnal convection over
1323 land. *J. Atm. Sci.*, **68**, 1041-1057.
1324

1325 Schlemmer, L., C. Hohenegger, J. Schmidli, and C. Schär, 2012: Diurnal equilibrium
1326 convection and land surface-atmosphere interactions in an idealized cloud-resolving
1327 model. *Quart. J. Royal Meteor. Soc.*, **138**, 1526-1539.
1328

1329 Segal, M., R. Avissar, M. C. McCumber, and R. A. Pielke, 1988: Evaluation of vegetation
1330 effects on the generation and modification of mesoscale circulations. *J. Atm. Sci.*, **45**,
1331 2268-2292.
1332

1333 Sen Roy, S., R. Mahmood, D. D. S. Niyogi, M. Lei, S. A. Foster, K. G. Hubbard, E. Douglas, and
1334 R. A. Pielke Sr., 2007: Impacts of the agricultural Green Revolution induced land use
1335 changes on air temperatures in India. *J. Geophys. Res.*, **112**, D21108,
1336 doi:10.1029/2007JD008834.
1337

1338 Sen Roy, S., R. Mahmood, A. Quintanar, and A. Gonzalez, 2011: Impacts of irrigation on dry
1339 season precipitation in India. *Theor. Appl. Clim.*, **104**, 193-207.
1340

1341 Shukla, S. P., M. J. Puma, and B. I. Cook, 2014: The response of the South Asian Summer
1342 Monsoon circulation to intensified irrigation in global climate model simulations.
1343 *Clim. Dyn.*, **42**, 21-36.
1344

1345 Singh, D., S. P. McDermid, B. I. Cook, M. J. Puma, L. Nazarenko, and M. Kelley, 2018: Distinct
1346 influences of land cover and land management on seasonal climate. *J. Geophys. Res.*,
1347 **123**, 12,017-12,039.
1348

1349 Suarez, A., R. Mahmood, A. I. Quintanar, A. Beltran-Przekurat, and R. A. Pielke Sr.,
1350 2014: A comparison of the MM5 and the Regional Atmospheric Modeling System
1351 simulations for land-atmosphere interactions under varying soil moisture. *Tellus A: Dyn.*
1352 *Meteor. Ocean.* **66**, 21486, <http://dx.doi.org/10.3402/tellusa.v66.21486>.
1353
1354

1355 Szilagyi, J., and T. E. Franz, 2020: Anthropogenic hydrometeorological changes at a regional
1356 scale: observed irrigation-precipitation feedback (1979-2015) in Nebraska,
1357 USA. *Sustain. Water Resour. Manag.*, **6**, 1. <https://doi.org/10.1007/s40899-020-00368-w>
1358

1359 Wei, J., P. A. Dirmeyer, D. Wisser, M. C. Bosilovich, and D. M. Mocko, 2013: Where does
1360 the irrigation water go? An estimate of the contribution of irrigation to precipitation using
1361 MERRA. *J. Hydrometeor.*, **14**, 275-289.
1362

1363 Winchester, J., R. Mahmood, W. Rodgers, F. Hossain, E. Rappin, J. Durkee, and
1364 T. Chronis, 2017: A Model-based assessment of potential impacts of man-made
1365 reservoirs on precipitation. *Earth Inter.*, **21**, 1-31.
1366

1367 Xu, Z., R. Mahmood, Z-LYang, C. Fu, and H. Su, 2015: Investigating diurnal and seasonal
1368 climatic response to land use and land cover change over monsoon Asia with the
1369 Community Earth System Model. *J. Geophys. Res.*, **120**, 1137-1152. DOI:
1370 10.1002/2014JD022479.
1371

1372 Yang, Z., Y. Qian, Y. Liu, L. K. Berg, H. Hu, F. Dominguez, Ben Yang, Z. Feng,
1373 W. I. Gustafson Jr., M. Huang, and Q. Tang, 2019: Irrigation impact on water and energy
1374 cycle during dry years over the United States using convection-permitting WRF and a
1375 dynamical recycling model. *J. Geophys. Res.*, **124**, 11220–11241.
1376

1377 Zhang, T., R. Mahmood, X. Lin, and R. A. Pielke Sr., 2019: Irrigation impacts on minimum
1378 and maximum surface moist enthalpy in the Central Great Plains of the USA. *Wea.*
1379 *Clim. Extr.* **23**, 100197.
1380
1381